

UNIVERSITY OF BELGRADE
FACULTY OF MATHEMATICS



Nikola Grulović

TECHNIQUES OF DATA AUGMENTATION
AND DATA CREATION FOR OBJECT
DETECTION

Master thesis

Belgrade, 2022.

Mentor:

dr Milena VUJOSEVIC JANIĆIĆ, associate Professor
University of Belgrade, Faculty of Mathematics

Members of the commission:

dr Mladen NIKOLIĆ, associate Professor
University of Belgrade, Faculty of Mathematics

Lester de ABREU FARIA, Professor at ITA & PHD in Microelectronics
IPFacens, Sorocaba, São Paulo, Brazil

Date of defense: _____

Master's thesis title: Techniques of data augmentation and data creation for object detection

Abstract: Automatic detection and recognition of objects has a very important role in everyday life. One of the most significant examples of the use of object detection and recognition is in autonomous driving. To enable efficient object recognition, machine learning methods are used, for example neural networks, deep learning and computer vision. However, to obtain results of the desired quality, a large amount of data, high processing power, and data labeling are usually required, which can be very expensive or largely unavailable. This thesis deals with methods for expanding the data, as well as methods for reducing the time needed to train the model, in case a large amount of data or a large processing power is not available. In the thesis, the data is expanded with standard augmentations and methods of creating new synthetic data. Using transfer learning reduces the time it takes neural networks to learn the main features of the available data. By using the mentioned methods, improved results are obtained compared to the current best model for object detection. Improved model is able to detect between 10% and 40% more instances depending on the class, and one new whole class, which were not detectable previously.

Keywords: artificial intelligence, machine learning, computer vision, deep learning, digital image, VGG16, YOLO, StyleGAN

Contents

1	Introduction	1
2	Object detection	3
2.1	The development of object detection	3
2.2	Object classification model VGG16	4
2.3	Object detection model R-CNN	5
2.4	YOLO object detection model	6
3	Dataset Expansion Techniques	7
3.1	The Small Data Set Problem	7
3.2	Standard augmentation methods	7
3.3	Generative adversarial networks	13
3.4	Transfer learning	18
4	Model evaluation techniques	19
4.1	Intersection over Union	19
4.2	Confusion matrix for object detection	19
4.3	Precision, recall and F_1 -score	21
4.4	Mean Average Precision	22
4.5	Fréchet inception distance	23
5	Implementation and results	24
5.1	Available data	24
5.2	Creating Synthetic Data	26
5.3	Model for object detection and prediction VGG16	35
5.4	YOLO object detection and prediction model	39
5.5	Comparative analysis of results	56

CONTENTS

6 Conclusion	57
Bibliography	59

Chapter 1

Introduction

Machine learning refers to the ability of a machine to draw conclusions using available data instead of strictly defined and coded rules. In fact, machine learning allows computers to learn by themselves. The results of machine learning indirectly occur in everyday life, from predicting the weather forecast to autonomous driving.

Supervised machine learning techniques involve the use of large amounts of labeled data. However, there are several reasons why large amounts of labeled data are not always available. Collecting and labeling data is a process that can be extremely expensive or even impossible [1]. For example, in the medical field, labeling data by radiology experts is expensive and not feasible on a large scale [2]. In such situations, machine learning has only a small amount of data at its disposal and it is necessary to apply special techniques and approaches in order to overcome the problem of availability of a small amount of data, if possible.

In this thesis, the problem of the availability of a small amount of data is solved, where the data are images with marked frames of objects. To solve the problem of a small amount of data, two approaches are used: expanding the data set and learning with the transfer of knowledge. The thesis describes the process of expanding the data set, whereby the data is expanded with standard transformations for image augmentation and with data obtained using a model for generating synthetic images. Expanding the data set using the above methods still does not solve the problem of small amount of data well enough.

The thesis also describes a technique transfer learning [3] on an already trained object detection model [4]. Using transfer learning aims to use learned knowledge from one domain to better learn in another [5]. An indirect contribution of using transfer learning is the reduction of processing power required for model training. By

CHAPTER 1. INTRODUCTION

using the mentioned methods of expanding the data set and learning with knowledge transfer, a model with better features is obtained.

The ideas presented here are based on previous research. In some studies where small amounts of data were available, using standard image transformations, new images were generated that were used in model training and that positively influenced the final results [6]. In addition, the generation of new images by generative adversarial networks is proposed to expand the data set in order to increase performance [6, 7]. Training generative adversarial networks with a small amount of data does not give satisfactory results [6], so the emergence of the differentiable augmentation method for generative adversarial networks [8] creates the possibility of generating new data using a small data set. The aim of this thesis is to expand the data set by standard image transformations and generate synthetic data by generative adversarial networks with a small amount of data, which were not previously in focus and which became available through the differentiable augmentation method.

In the chapter 2, a brief overview of the object detection model used in this thesis is given. Chapter 3 gives an overview of techniques and generative adversarial networks used in solving problems of small amount of data, while chapter 4 describes the evaluation techniques of those models. Experiments and results of the obtained models are presented in the chapter 5. In the chapter 6, the problems faced by this work, methods of overcoming them and possible further improvements of the solution are briefly presented.

Chapter 2

Object detection

Computer vision is a field of machine learning, which deals with the construction and use of systems for processing, analysis and interpretation of digital images or videos [9, 10]. Object detection is a computer vision technique whose task is to detect objects in an image. For successful object detection, it is necessary to train the model on a large amount of data. As it is sometimes impossible to obtain a sufficient amount of data, data augmentation is used: the data is expanded by adding modified or synthetically generated data [11].

2.1 The development of object detection

Object detection is used in a large number of applications, such as, for example, autonomous driving, robotic vision, video surveillance, etc. [12]. In the last two decades, progress in object detection has gone through two periods [12]: the “traditional object detection period” (before 2014 year), and the “deep learning-based object detection period” (after 2014).

The performance of object detection has been significantly improved thanks to deep convolutional neural networks (CNN), which has led to remarkable discoveries. The development of a deep convolutional neural network also enabled the detection of bounding boxes¹ and significant parts of the object in the images [13, 14, 15, 16]. In the era of deep learning, object detection can be grouped into two types: *two-stage detection* and *one-stage detection* [12].

¹Bounding boxes represent coordinates on part or the whole image within which the recognized object is located.

Within two-stage detection, the first stage of the model is used to extract regions², while the second stage is used to classify and further refine objects. This method of object detection is relatively slow, but gives very precise results.

One-stage object detection models refer to a class of models that skip the region proposal stage. Such models require only one pass through the neural network and predict all bounding boxes in one pass at the end. This type of model usually has faster detection, but is less accurate in detecting and recognizing objects.

2.2 Object classification model VGG16

The VGG16 model uses CNN and was considered one of the best computer vision models in 2014 after winning the ILSVR (Imagenet) contest [17]. The authors of this model looked at other models and noticed that by increasing the depth and using an architecture with smaller convolutional filters, performance can be improved. The change in architecture proved to be a significant improvement over previous models [17].

The VGG16 model belongs to the single-stage detection model and got its name from the sixteen layers that can learn, while the entire network consists of thirteen convolutional layers, five max pooling layers and three fully connected layers that are summed up in a total of twenty-one layers. The architecture of the VGG16 model is given in the figure 2.1.

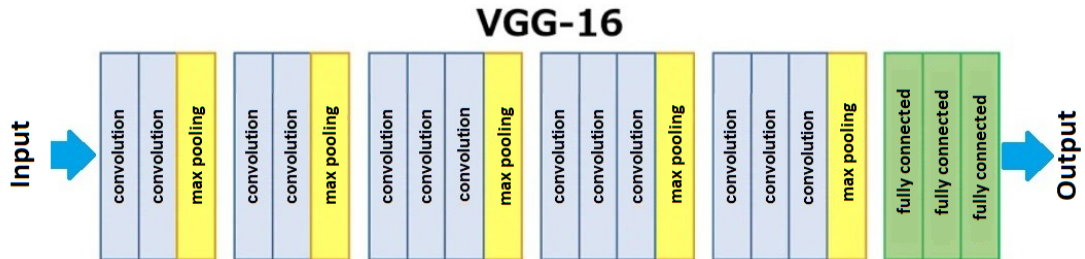


Figure 2.1: VGG16 architecture

The model was able to predict the objects in the given images with a classification error of 6.8% on the test set, outperforming the first subsequent model by 0.9% [17]. Test set of ILSVR contained 40152 images, which was around 10% of total amount of images contained in dataset [18]. The disadvantage of the VGG16 model is that it is not able to determine the frames of the detected object in the image.

²Regions represent parts of the image that may contain objects or parts of objects

2.3 Object detection model R-CNN

Due to the reuse of convolutional neural networks and the greater computing power available, in 2014 a model named regions with CNN features (R-CNN) appeared in 2014 [13]. The R-CNN model is the first two-stage detection model and consists of three modules that perform different tasks [13]:

1. The first module generates region suggestions using a selective search algorithm. The selective search algorithm performs image segmentation based on pixel intensity using a graph-based segmentation method [19]. Based on the obtained segmentation map, suggestions of regions are created that are used in the next module [20].
2. The second module is a large convolutional neural network. Each proposal is scaled to a fixed-size image and fed into a trained CNN model to extract a fixed-length feature vector.
3. The third module is a set of linear methods of support vector machines specific for each class, which recognize objects from the vector of features.

The problems that arise with R-CNN are [21]:

- Due to the possible classification of a large number of region proposals per image, model training cannot be used in real time.
- The selective search algorithm is fixed and as such does not adapt to the data. This can result in poor region proposals being obtained in some situations.

During several iterations of the development of R-CNN, the model is significantly accelerated and new models are created: fast R-CNN [22] and faster R-CNN [14]. The fast R-CNN object detection model takes a similar approach to R-CNN with a few simple improvements to the model. The faster R-CNN object detection model is composed of two modules. The first module is a deep convolutional network that proposes regions, while the second module is an R-CNN model that uses proposed regions for object recognition. The entire system is a single, unified object detection network [14].

2.4 YOLO object detection model

The object detection model R-CNN uses regions to detect objects within an image. The model does not look at the complete image, but instead looks at parts of the image that have a high probability of containing objects. You only look once, YOLO for short, is an object detection model that differs from region-based models. The YOLO model belongs to the model based on one-stage detection and was created in 2015 [23]. With the YOLO model, a single convolutional network predicts regions and detects objects in bounding boxes.

Separate components of object detection are combined into one neural network. The model uses the found features from the whole image to predict each bounding box. Also, all bounding boxes for all objects in the image are predicted simultaneously. This means that the model thinks globally about the entire image and all the objects on it [23]. YOLO model two times as fast compared to faster R-CNN, and has 5% better accuracy. Comparison of models is presented on figure 2.2 [24].

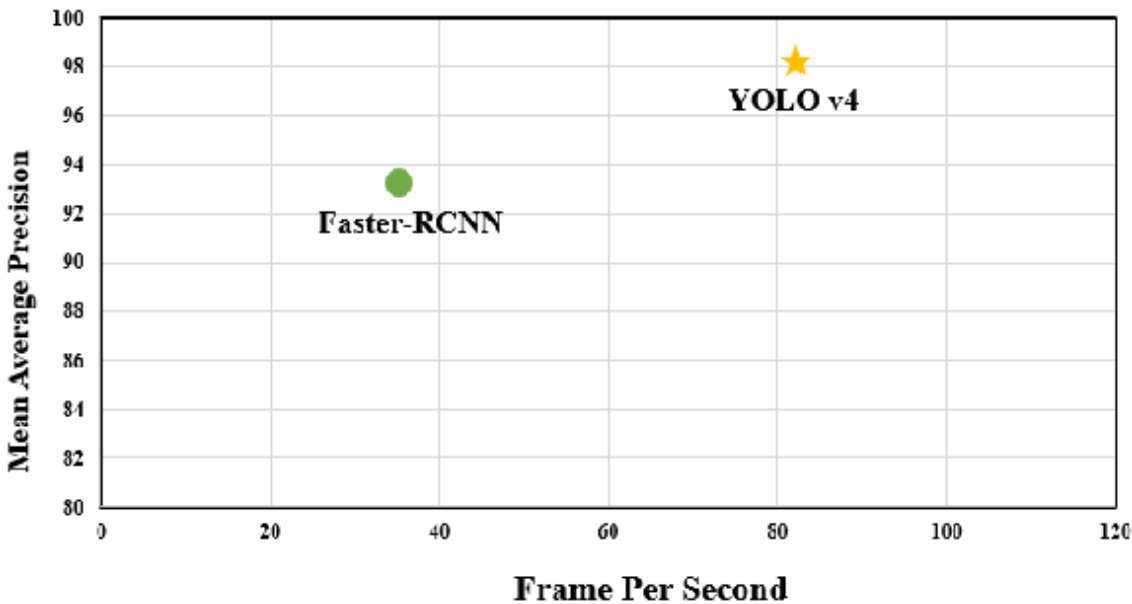


Figure 2.2: Comparison of YOLO model with faster R-CNN model [24]

Chapter 3

Dataset Expansion Techniques

The dataset can be expanded by creating new data. Data creation techniques include data augmentation and generative adversarial networks. In some cases, even after expanding the training set, the amount of data available may be insufficient to train the model. Such a problem can be alleviated by the transfer learning technique.

3.1 The Small Data Set Problem

Models trained on a small dataset tend to find features that do not exist, resulting in high variance and high error on the validation set. In this thesis, two methods are used to avoid this behavior. The first method is to expand the dataset. The data is augmented with images that have been altered using standard augmentation methods and images that have been synthetically generated using generative adversarial networks. Another method is the use of transfer learning.

3.2 Standard augmentation methods

Standard augmentation methods include rotation, flip, scale, crop, blur and color augmentations. Randomly combining the mentioned methods creates new data that serves as an extension of the training dataset.

Flip

Image flipping refers to the creation of a new image that corresponds to the mirror image, with respect to the vertical or horizontal axis. It is not possible to

apply the flipping operation in every domain. For example, vertical flipping will not make much sense in the case of traffic vehicles. Examples of flipping are shown in the figure 3.1.



Figure 3.1: Flipping example: original image (left), vertical flipping (middle) and horizontal flipping (right) [25]

Rotation

Rotation is a transformation that creates new images that correspond to the original image rotated by an arbitrary angle. By applying the rotation operation, the dimensions of the image are often changed. If it is necessary to preserve the original dimensions, the image is cut as necessary, while the empty parts of the image are filled using a certain method. Examples of rotations are given in the figure 3.2.



Figure 3.2: Rotation example: original image (left), 45° rotation (middle) and 120° rotation (right) [25]

Scaling

Scaling is a transformation that increases or decreases the image by a given factor that is greater than zero. When using a scaling factor greater than one, the dimensions of the final image are larger than the original. To preserve the original dimension, the new image is cropped to the original dimension. In case the scaling factor is between zero and one, the dimensions of the image are smaller than the original. In order to preserve the original dimensions, the empty space is filled using a certain method. Examples of scaling are given in figure 3.3.



Figure 3.3: Scaling example: original image (left), scale factor greater than 1 (middle) and scale factor between 0 and 1 (right) [25]

Cropping

Cropping an image refers to creating a new image by randomly sampling parts of the original image. The crop is then scaled to the dimensions of the original image. An example of cropping is given in the figure 3.4.



Figure 3.4: Crop example: original image (left), random crop (middle and right) [25]

Translation

Translation means moving the image in a horizontal or vertical direction. This method is very useful, because most objects can be located anywhere in the image. The empty space that is created after the transfer is painted using appropriate methods. An example of translation is shown in the figure 3.5.



Figure 3.5: Translation example: original image (left), random translation (middle and right) [25]

Gaussian noise

Gaussian noise is the addition of random values from a normal distribution to the pixels of the original image. This creates a new image with noise. By adding Gaussian noise, all features in the data are deformed. This is important because there may be data in the training dataset that contain similar features, which can lead to overfitting of the model being trained on that set. An example of noise is given in the figure 3.6.



Figure 3.6: Example of adding noise: original image (left), mean 1 and standard deviation 0.1 (middle), mean 0 and standard deviation 0.5 (right) [25]

Gaussian blur

Gaussian image blur is an application of a convolution operation¹ with a Gaussian bell [26]. Increasing the standard deviation produces a stronger blurring effect. An example of blur is shown in the figure 3.7.



Figure 3.7: Blur example: original image (left), standard deviation 7 (middle), standard deviation 21 (right) [25]

Color Augmentation

Color augmentation changes the color properties of an image by changing the values of its pixels. Pixel values can be changed in different ways.

Brightness involves multiplying each pixel of the image by the corresponding illumination factor greater than zero. If the brightness factor is between zero and one, a darker image is obtained, and if it is greater than one, a brighter image is obtained. An example of brightness is shown in the figure 3.8.



Figure 3.8: Example of changing brightness, original image (left), brightness factor between 0 and 1 (middle), brightness factor greater than 1 (right) [25]

¹convolution is an operation on two functions f and g that produces a third function $f * g$, which expresses how the shape of one is modified by the other

CHAPTER 3. DATASET EXPANSION TECHNIQUES

The technique of changing the contrast represents changing the degree of difference between the lighter and darker parts of the image. Increasing the contrast increases the difference between brighter and darker parts, while decreasing the contrast decreases the difference. An example of changing the contrast is shown in the figure 3.9.



Figure 3.9: Example of contrast change, original image (left), example of enhanced contrasts (middle and right) [25]

The technique of changing saturation of the image represents changes in the saturation of colors. By increasing the saturation, an image with more pronounced colors is obtained. An example of saturation change is shown in the figure 3.10.



Figure 3.10: Example of saturation change, original image (left), weaker increase in saturation (middle), stronger increase in saturation (right) [25]

The technique of changing the HUE moves the pixels in the image to another point on the color wheel. Random displacement generates new images with different colors. An example of a shade change is shown in figure 3.11.



Figure 3.11: Example of hue change, original image (left), shifted pixels for random values (middle and right) [25]

3.3 Generative adversarial networks

During the development of machine learning, the concept of generative adversarial networks (GAN) was developed. In generative adversarial networks, there are two models: *generator* and *discriminator*. The generator is tasked with generating images and the discriminator is tasked with distinguishing generator-generated images from real images [27]. The basic architecture of generative adversarial networks is shown in figure 3.12.

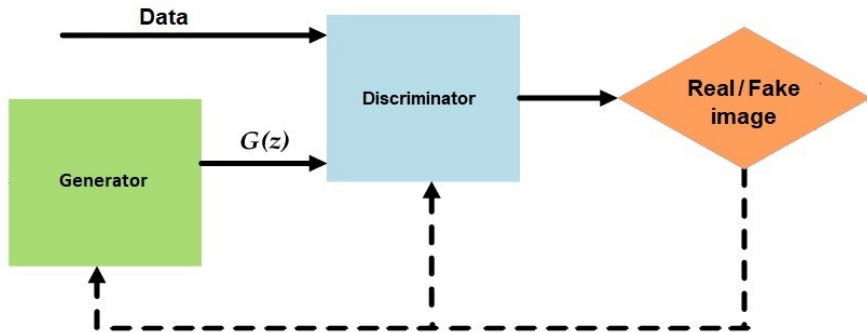


Figure 3.12: Generative adversarial networks: input data represent images, $G(z)$ is the image generated by the generator [28]

Generative adversarial networks rely heavily on large amounts of diverse and high-quality training data to generate photo-realistic images [8]. The generator is trained to generate images that the discriminator will not distinguish from real ones, while the discriminator is trained to distinguish fake images from real ones. As the

generator changes, so must the discriminator and vice versa. Thus, the generator and the discriminator are trained alternately [29]. Loss functions for generative adversarial networks can be formulated via a zero-sum game [30, 31]. The generator tries to minimize the function while the discriminator tries to maximize. For a given generator G and discriminator D , the zero-sum game problem is defined as [30, 29]:

$$\min_G \max_D \mathbb{E}_x[\log D(x)] + \mathbb{E}_z[1 - \log D(G(z))] \quad (3.1)$$

In the given formula:

- $D(x)$ represents the discriminator's estimate that the real data x is real,
- \mathbb{E}_x is the expectation from the distribution of real data,
- $G(z)$ is the output of the generator for the value z from the latent space,
- $D(G(z))$ represents the discriminator's estimate that the false data is real,
- \mathbb{E}_z is the expectation from the data distribution in the latent space.

Progressive generative adversarial networks modify the architecture in such a way that the training of generative adversarial networks starts with a low image resolution and then progressively increases the resolution by adding layers to the network. The training process is shown in the figure 3.13. This incremental nature allows the model during training to first detect visual features that manifest on the initial layers, from rough lines to fine details [32].

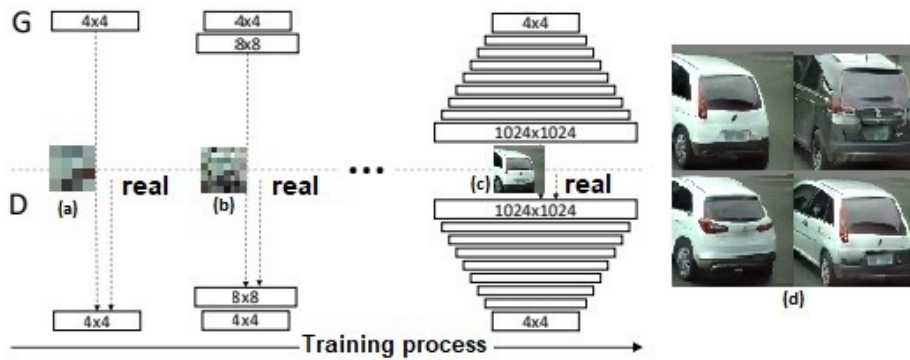


Figure 3.13: The training process of progressive generative adversarial networks starts from low resolution images (4×4) and progressively adds layers to the network and the resolution increases up to (1024×1024). The first image (image a) represents the first iteration of model training, the second image (image b) represents the second iteration of training, while the third image (image c) represents the last iteration. The car images (image d) represent the highest resolution generated images [32].

During the development of generative adversarial networks, most of the work was done on improving the discriminator, which led to better results. On the other hand, style generative adversarial network *StyleGAN* is an addition to the architecture of generative adversarial networks, which introduces significant modifications to the generator model [33].

The style-based model generator consists of two parts and is shown in figure 3.14. The first part forms a deeply connected network with eight layers. The network is represented as a function $f : Z \rightarrow W$ and is called a mapping network. The input of the network represents the normalized latent code $z \in Z$. Latent code or z-vector z , is a vector containing random values from the Gaussian distribution. The space in which all z-vectors are located is called Z-space and is denoted by Z . The output of the network is the vector w which belongs to the latent space W . Latent space is an abstract multidimensional space that contains characteristic values that cannot be directly interpreted. The second part of the generator is a network which, with the help of vectors with random values from the Gaussian distribution, random noise and the vector w transformed by an affine transformations generates an image.

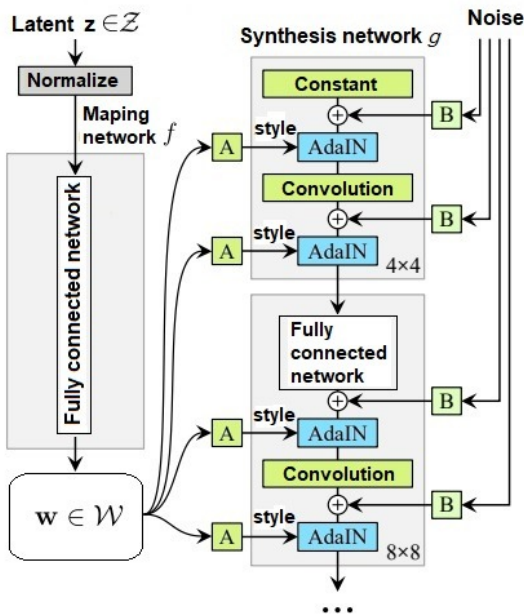


Figure 3.14: Style based generator model, “A” represents affine transformation while “B” represents the scaling factor for noise [33].

The vector w transformed by affine transformations serves to adjust the style of synthetically generated images using adaptive instance normalization (AdaIN). Image style represents a vector in latent space that is separated from the semantic content vector of the image [34]. An example of transferring a style from one image to another is given in the figure 3.15.

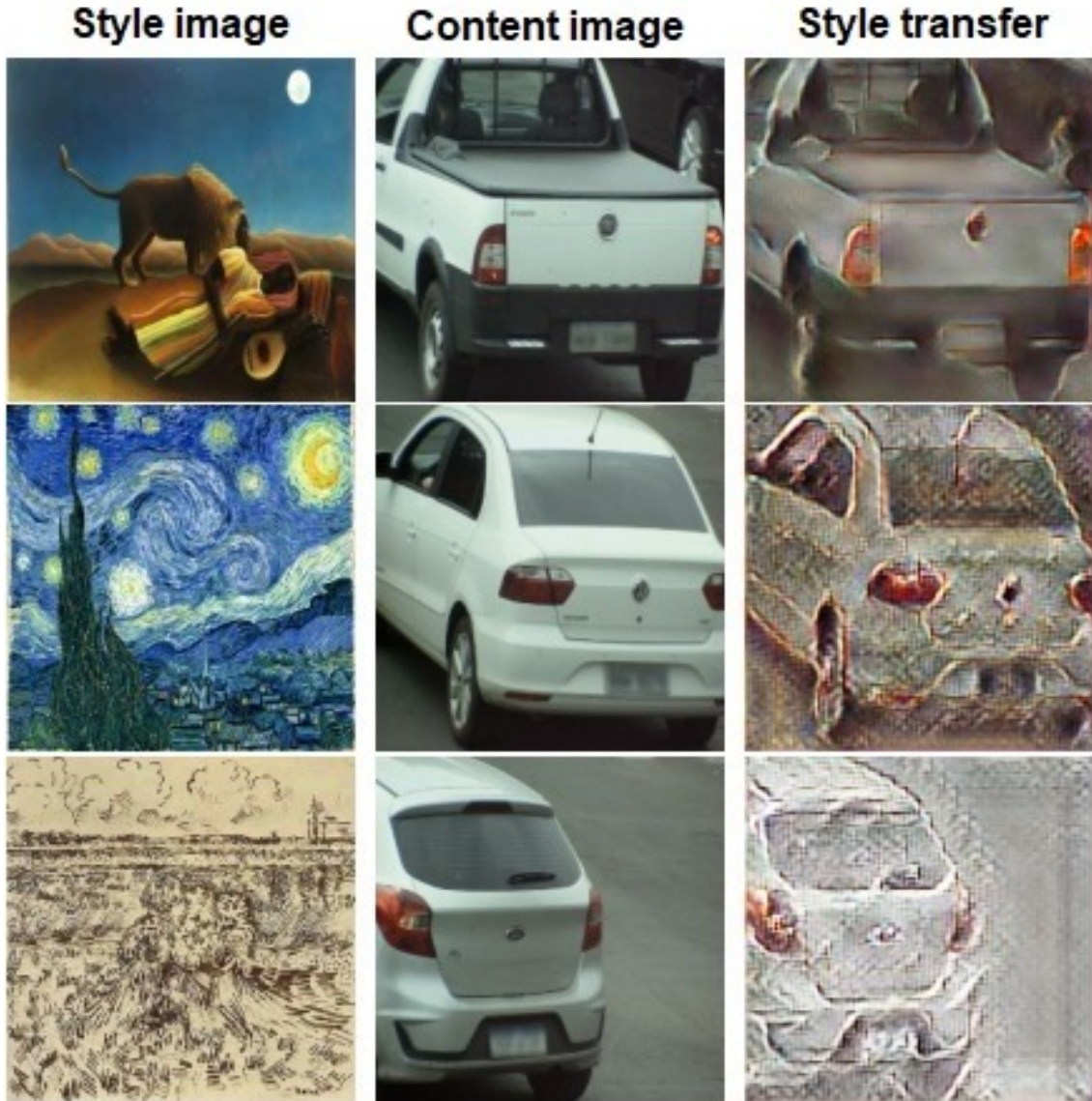


Figure 3.15: Transfer of styles to desired images and results of AdaIN operation [34].

The *StyleGAN* model generates photo realistic images. During development, the *StyleGAN* model went through a phase of optimization and minor changes to the synthesis network. The new version of *StyleGAN*, *StyleGAN2* brings up to 60%

faster model training compared to the first version [35]. Due to such speedups, the processing power required for training is reduced as well. The thesis uses this improved version, more precisely the *StyleGAN2* architecture.

Unless a large amount of data is available, working with generative adversarial networks can result in low-quality models. In order to alleviate such a problem, the method of differentiable augmentation was introduced for the *StyleGAN2* model. The method uses different types of augmentation on real and fake data. The method enables more stable training and leads to better convergence compared to training the model without the differentiable augmentation method over the same data set. The *StyleGAN2* model with the differentiable augmentation method is able to produce realistic images, even over a dataset containing only one hundred images [8].

3.4 Transfer learning

In supervised learning, models are trained to learn the connections between given inputs and outputs. The models can then make output predictions on the new data. In this way, models will perform well when solving a problem that is in the same domain as the training data. The result will deteriorate if the problem domain changes. In the worst case, it may be necessary to train a new model even when the problem domains are similar [3].

Transfer learning is a field of machine learning that deals with exploiting knowledge from an existing trained model when training a new model that should solve a similar task. The technique is most often used when there is not enough data or resources available to train a new model. Using transfer learning brings a number of advantages, the main of which are saving resources, reducing errors during training, and generalizing the model [3].

Chapter 4

Model evaluation techniques

For object detection model evaluation, the score of mean average precision (mAP) is used, which takes into account precision and recall. Also, a confusion matrix is used, where the calculation of correctly and incorrectly classified objects depends on the given threshold of the intersection over union metric (IoU) and the confidence score of classified objects. The confidence score represents the object's probability value that the model assigned to it during classification.

4.1 Intersection over Union

Intersection over Union is an evaluation metric used to measure the accuracy of object detectors. The picture 4.1 shows an example of a frame, where the predicted frame is drawn in red, while the real frame is drawn in yellow. The metric is calculated by dividing the intersection of two frames by their union (figure 4.2). On perfectly predicted bounding boxes, the IoU metric will give a value of 1.0, while if the bounding boxes do not intersect, the value will be 0. Ideal cases where the metric is 1.0 are rare, and in practice it is considered a good result when the IoU has a value of 0.8.

4.2 Confusion matrix for object detection

The confusion matrix is a tabular representation of the numbers of correctly and incorrectly classified objects, on the basis of which classification models can be evaluated. For multi-class classification of object detection, the confusion matrix is expanded by one column and one type. The new column serves to record the

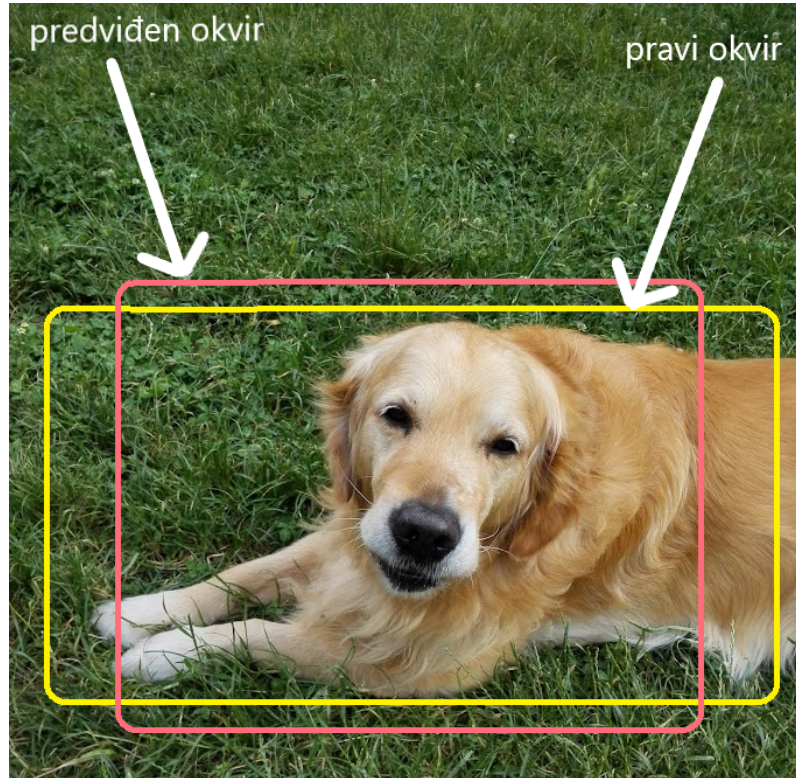


Figure 4.1: Predicted frame (red) and real frame (yellow) over given object

$$\text{IoU} = \frac{\text{Area of Overlap}}{\text{Area of Union}}$$

Figure 4.2: IoU metric calculation demonstration

number of objects that are classified in the image, but are not on it. The type is used to record the number of objects that are in the image, but are not classified. An object is classified correctly when it meets the following conditions:

- model correctly classified the object, ie. assigned him the right class,
- the value of the confidence score of the object exceeds the given threshold of the confidence score (usually 0.5 is used in practice) i

- IoU value of the object exceeds the given IoU threshold (usually 0.5 is used in practice)

If the object does not meet one of the given conditions, it is classified incorrectly.

The confusion matrix is also calculated for each class individually and is similar to binary classification. When calculating the confusion matrix, one specific class is observed and that class is considered positive, while the set containing all objects of the other classes is considered a negative class. An object is classified as positive if it meets the following conditions:

- object belongs to positive class the model assigned it a positive class,
- The object's IoU value exceeds the specified IoU threshold

If the object does not meet one of the given conditions, then it is assigned a negative class. The confidence score does not participate in the computation of the confusion matrix for each class.

True Positive (TP) is the number of objects that belong to the positive class, the model assigned them a positive class and the IoU value of each object exceeds the given IoU threshold.

True Negative (TN) is the number of objects that do not belong to the positive class and were assigned a negative class by the model. The IoU is not compared to the threshold.

False Positive (FP) is the number of objects that belong to the negative class but were assigned a positive class by the model. Also, it is the number of objects that belong to the positive class, but the IoU value of each object does not exceed the given IoU threshold.

False Negative (FN) is the number of objects that belong to the positive class and the model assigned them a negative class. The IoU is not compared to the threshold because the classification is wrong.

4.3 Precision, recall and F_1 -score

Precision is the percentage of truly positive objects among objects that are classified as positive and is defined by the formula:

$$Precision = \frac{TP}{TP + FP} \quad (4.1)$$

Higher precision also means that there are fewer false positive objects.

Recall represents the percentage of positive objects that are correctly classified and is defined by the formula:

$$Recall = \frac{TP}{TP + FN} \quad (4.2)$$

A high recall means that there are few false negative objects.

Precision and recall can be summed up in a score, which is called the F_1 -score [36] and is defined by the formula:

$$F_1 = 2 \frac{Precision \cdot Recall}{Precision + Recall} \quad (4.3)$$

F_1 -score is the harmonic mean of precision and recall and it discourages hugely unequal values and extremely low values. F_1 -score to give a reasonably low score when either precision or recall is low and only harmonic mean enables that.

Macro-averaged F_1 -score is calculated as an arithmetic mean:

$$F_{1avg} = \frac{1}{n} \sum_{k=0}^{k=n-1} F_{1k} \quad (4.4)$$

where F_{1k} is the value of the F_1 -score for the k th class. The macro-averaged F_1 -score is computed using the arithmetic mean of all the per-class F_1 -scores and it is used to assess the quality of problems with multiple binary labels or multiple classes.

The Weighted-averaged F_1 -score is calculated by the following formula:

$$F_{1wavg} = \sum_{k=0}^{k=n-1} (F_{1k} S_k) \quad (4.5)$$

where F_{1k} and S_k are the value of the F_1 -score for the k th class and the proportional number of instances of the k -th class in relation to the total the number of instances in the dataset.

4.4 Mean Average Precision

Average precision is a method of calculating the area under the precision and recall curve for one class. Precision and recall values are calculated for given values of IoU thresholds from the interval [0.5 to 1.0), most often with a step of 0.05. The range of calculated recall and precision values is supplemented by **0** and **1**, respectively.

Average precision is calculated using the following formula:

$$AP = \sum_{k=0}^{k=n-1} (R_k - R_{k+1})P_k \quad (4.6)$$

where R_k and P_k are the recall and precision for the k th IoU threshold. R_k

The mean average precision is calculated as the mean value of all the average precisions given by the formula:

$$mAP = \frac{1}{N} \sum_{i=1}^N AP_i \quad (4.7)$$

where N represents the number of classes and AP_i the average precision for a class i .

4.5 Fréchet inception distance

Fréchet inception distance (FID) is a metric used to evaluate the quality of images generated by generative adversarial networks [37]. The Fréchet inception distance compares the distribution of the generated images to the distribution of the actual images that were used to train the generator. The Fréchet inception distance for two identical images gives a value of zero, while for different ones it gives a number greater than zero.

The Fréchet inception distance is calculated for two joint normal distributions $\mathcal{N}(\mu, \Sigma)$ and $\mathcal{N}(\mu', \Sigma')$ by the following formula [38, 37]:

$$d_F(\mathcal{N}(\mu, \Sigma), \mathcal{N}(\mu', \Sigma'))^2 = \|\mu - \mu'\|_2^2 + \text{tr} \left(\Sigma + \Sigma' - 2 \left(\Sigma^{\frac{1}{2}} \cdot \Sigma' \cdot \Sigma^{\frac{1}{2}} \right)^{\frac{1}{2}} \right) \quad (4.8)$$

In practical use, image distributions are obtained by computing mean values (μ, μ') and covariance matrices (Σ, Σ') using the vectors obtained by the model *InceptionV3*¹.

¹InceptionV3 is a convolutional neural network used for image analysis and object detection.

Chapter 5

Implementation and results

As part of the implementation, the available dataset is expanded with augmentation methods and synthetic data generated by the *StyleGAN2* model. In order to assess whether the applied techniques enable improvement, the model is trained on the basic data set and compared with the models trained on the extended data set. The code developed as part of the thesis work is available at [github¹](#) [39]. The data used in this work, as well as the generated data, are available at [this address²](#) [40]. The [Google Colab³](#) platform was used for model training. The platform provided an NVIDIA Tesla P100-PCIE graphics card with 16GB of RAM memory.

5.1 Available data

BRAIN Institute (eng. *Brazilian Artificial Intelligence Nucleus*), within the FACENS⁴ faculty (pt. *Centro Universitário FACENS*, eng. *Faculty of Engineering of Sorocaba*) Sao Paulo, Brazil provided an annotated dataset, called BVS (*Brazilian vehicle set, BVS*), which was used in this thesis. The dataset BVS contains four classes: *car*, *motorbike*, *truck* and *bus*. Examples from these classes are shown in the figure 5.1. The total amount of data is 1872 images, most of which belong to the *car* and *motorbike* classes. In the dataset BVS, the resolution of all images is 800×600px.

¹<https://github.com/Grula/vehicle-detection>

²<https://drive.google.com/file/d/1EkrO28-iBCVWYPqy5mJXn8P8EoKQ6xUH/view?usp=sharing>

³<https://research.google.com/colaboratory>

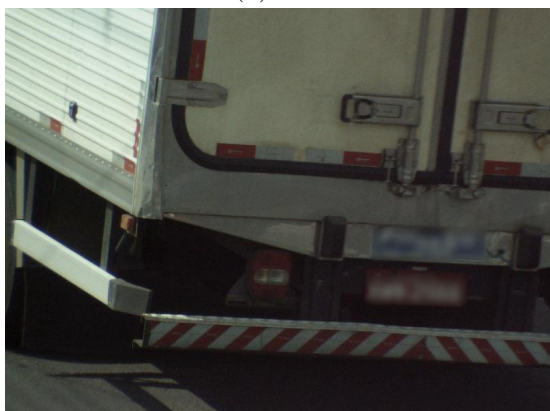
⁴(www.facens.br)



(a) *car*



(b) *motorbike*



(c) *truck*



(d) *bus*

Figure 5.1: Examples of images from available classes

The images are divided into two sets, a training set and a test set for the model. 10% images from each class were randomly taken for the test set. The test set did not participate in any augmentation techniques and was not used in any way in model tuning. The total number of images of each class, the number of images belonging to the training set and the number of images belonging to the test set are shown in the table 5.1. From the table 5.1 it can be seen that the imbalance between the classes is extremely high, even 1:15 between the classes *bus* and *car*.

Table 5.1: The total number of images for each class, and the number after splitting into a training set and a test set

class	total number	training set	test set
car	889	800	89
motorbike	966	869	97
truck	10	9	1
bus	7	6	1

5.2 Creating Synthetic Data

The training set was augmented in two ways: images were generated by standard augmentation transformations and the *StyleGAN2* model. Table 5.2 shows the exact number of images that were generated in order to obtain balanced classes, more precisely that each class contains an equal number of images in the training set. The number of images chosen to expand the training set was chosen based on the class that contained the largest amount of data, specifically the *motorbike* class. The *motorbike* class is expanded with 869 images, more precisely with as many images as are present in the training set. After expanding the training set, each class contains 1738 images.

Table 5.2: Total number of generated images

class	car	motorbike	truck	bus
number of images generated	938	869	1732	1729

Generating data with standard image transformations

Due to the need to expand the data set BVS, new data are generated by augmentation techniques (chapter 3.2). The expanded set is called BVSstandard further on in the thesis. The set of augmentations that are applied are:

- reflection — is performed only in the horizontal direction and care is taken to change the coordinates of the border frames,
- rotation — done with a random angle between one and five degrees and the empty space is filled with border pixel colors,
- translation — moves the image in a random direction by ten pixels and the empty space is filled with the colors of the border pixels,
- Gaussian noise — pixels from the image are mapped to the interval -1 to 1 and noise with constant standard deviation 0.1 and mean value 0 is added to them, after addition the pixels are returned to the interval 0 to 255.
- Gaussian Blur — is applied to the image with a constant standard deviation of 7. The standard deviation value is chosen because of the resolution of the images in the BVSset. Using a value of 7 for the standard deviation blurs the images while still making it possible to recognize the object in the image.
- color augmentation — The brightness parameter is randomly selected from a uniform distribution from the interval 0.5 to 1.5. Contrast, saturation and hue parameters are randomly selected from a uniform distribution from the interval 0.0 to 10.0. Intervals of color augmentation sin chosen after testing intervals of different ranges. It was concluded that the best results are obtained using the specified intervals.

Four randomly chosen augmentations are applied from the described set of augmentations. One affine transformation is chosen at random from the set consisting of reflection, rotation and translation. Also, one augmentation is chosen between Gaussian blur and Gaussian noise. From the set of color augmentations that make up brightness, contrast, saturation, and hue, two augmentations are randomly selected. Examples of generated images are shown in figure 5.2.



Figure 5.2: Examples of images generated by standard transformations

Data generation with the *StyleGAN2* model

The data set BVS is also extended with synthetic data generated by the *StyleGAN2* model. The name BVSstyle is used for this extended set in the thesis.

However, the problem of small amount of data also occurs for the generation of new images by the *StyleGAN2* model. Using the differentiable augmentation method outlined in section 3.3 overcomes the problem of small amount of data and the model successfully generates images. The implemented differentiable augmentation method was tested on the CIFAR-10 data set [41].

The *StyleGAN2* model architecture is implemented using the *Tensorflow* 2.0 library⁵. The generated images are 512×512 in size. This dimension was chosen due to memory limitations of the graphics card. Model training lasted twelve to forty-eight hours, depending on the class itself. Every six hours of training or, more precisely, every twenty-five thousand epochs, a checkpoint was made. After each checkpoint, images were generated to calculate the Fréchet inception distance.

The Fréchet inception distance metric and Loss function for generative adversarial networks were used to evaluate the *StyleGAN2* model. After each checkpoint, Fréchet inception distance was used to assess the similarity between the two sets of images: the images generated by the model were compared to the real images from the test set BVS. The calculation of the Fréchet inception distance took place on an NVIDIA 780Ti graphics card and took a total of ten minutes. When an object could be recognized in the generated image and when the Loss function of the discriminator and generator did not decrease significantly, further training of the model was stopped. The exact number of epochs of each class is given later in the text.

Classes *Bus* and *Truck*

Training the *StyleGAN2* model on the *truck* and *bus* classes was a big challenge due to the small amount of available data. The training of the model lasted twenty-four hours. Two hundred thousand images were generated for model training using the differentiable augmentation method. The original training image set for the *bus* class contained six images, and the training set for the *truck* class contained nine images.

⁵The *Tensorflow* 2.0 library is open source and provides a comprehensive ecosystem of tools. It was published in 2015 by the *Google Brain* team. The main purpose is to create machine learning models. The library is intended for use in the programming language *Python*.

For the *truck* class the Loss function is given in figure 5.3 and the result of the Fréchet inception distance for the two checkpoints is given in table 5.3. From the Loss function for the discriminator, it can be seen that the discriminator could have improved with further training. Increase from discriminator means that generator started generating images that discriminator had difficult time to distinguish from real ones. From the images generated by the final weights of the model, it is possible to observe the main features of the objects. As the objects in the picture can be recognized and to save resources, the training was stopped. Examples of generated images of the *truck* class are shown in the figure 5.4.

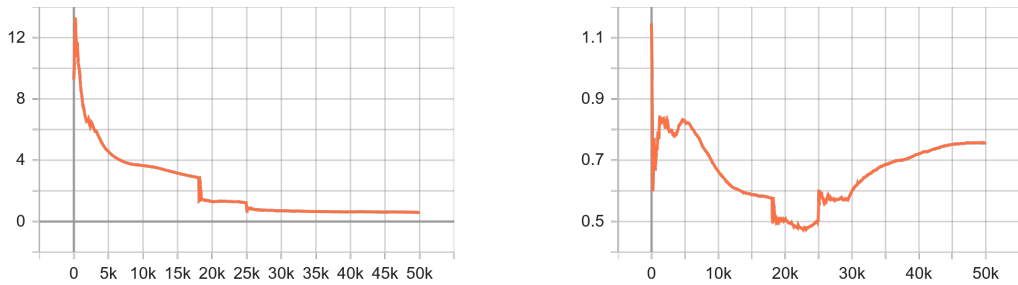


Figure 5.3: Loss functions for the class *truck*, generator (left) and discriminator (right). In both cases, the x axis represents the epochs, while the y axis represents the values of the corresponding Loss function.

Table 5.3: Class *truck*

epoch number	Fréchet inception distance
25 thousand	432.8
50 thousand	188.5

For the class *bus* from the Loss function (image 5.5) and the results of the Fréchet inception distance (table 5.4) it can be concluded that further training for the next twenty five thousand epochs does not they get significantly better results. Examples of generated images of the *bus* class are shown in the figure 5.6.

Table 5.4: Class *bus*

epoch number	Fréchet inception distance
25 thousand	369.2
50 thousand	220.5



Figure 5.4: Examples of generated images of the *truck* class

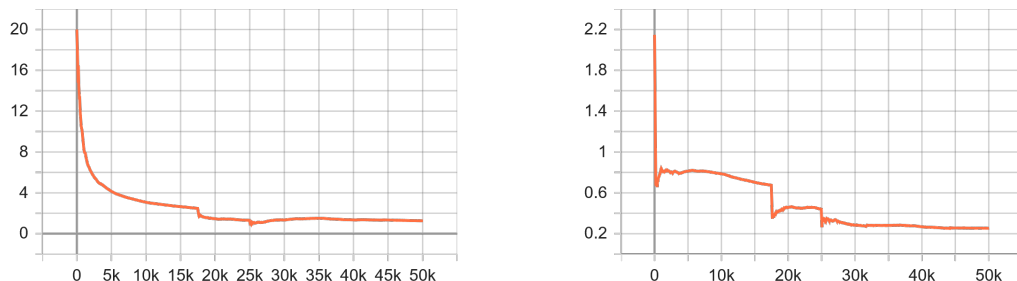


Figure 5.5: Loss functions for class *bus*, generator (left) and discriminator (right). In both cases, the *x* axis represents the epochs, while the *y* axis represents the values of the corresponding Loss function.



Figure 5.6: Examples of generated class images *bus*

Classes *car* and *motorbike*

The training of the model over the *car* class lasted about thirty-six hours and three hundred thousand images were generated using the differentiable augmentation method. For the *car* class, the Loss function is shown in figure 5.7. The result of the Fréchet inception distance is shown in table 5.5. Further training of the *car* class does not result in significant improvements to the model. Examples of generated images of the *car* class are shown in the figure 5.8.

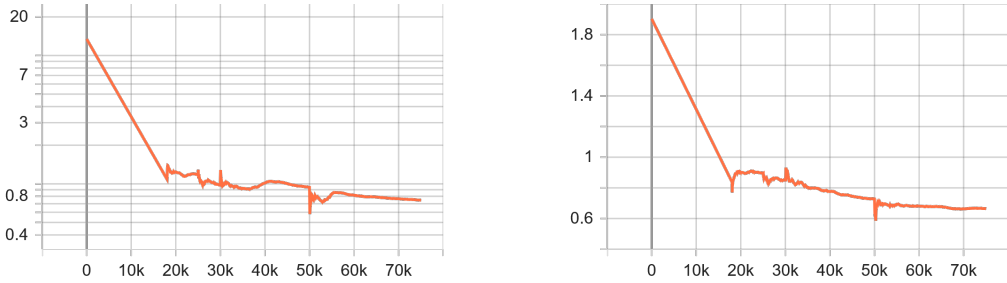


Figure 5.7: Loss functions for the *car* class, generator (left) and discriminator (right). In both cases, the x axis represents the epochs, while the y axis represents the values of the corresponding Loss function.

Table 5.5: Class *car*

epoch number	Fréchet inception distance
25 thousand	107.6
75 thousand	87.5



Figure 5.8: Examples of generated class images *car*

The training for the *motorbike* class lasted forty-eight hours and four hundred thousand images were generated using the differentiable augmentation method. The *motorbike* class has slightly worse results with the Loss function shown in figure 5.9. The generator's Loss function is increasing, indicating that the discriminator is getting much better at distinguishing real from fake images. The images generated by the generator are not perfect, but it is possible to recognize the main features of objects that are important for training object detection models. The result of the Fréchet inception distance (table 5.6) indicates that during training there is an improvement in the generated images. Examples of generated images of the *motorbike* class are shown in figure 5.10.

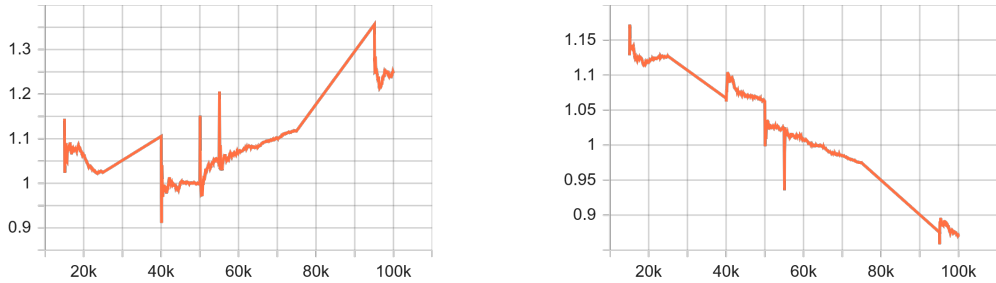


Figure 5.9: Loss functions for class *motorbike*, generator (left) and discriminantator (right). In both cases, the x axis represents the epochs, while the y axis represents the values of the corresponding Loss function.

Table 5.6: Class *motorbike*

epoch number	Fréchet inception distance
25 thousand	386.8
100 thousand	151.1

The generated images are not perfect, but it is possible to recognize the main features of the objects. Some generated images are prone to artifacts and blurs.

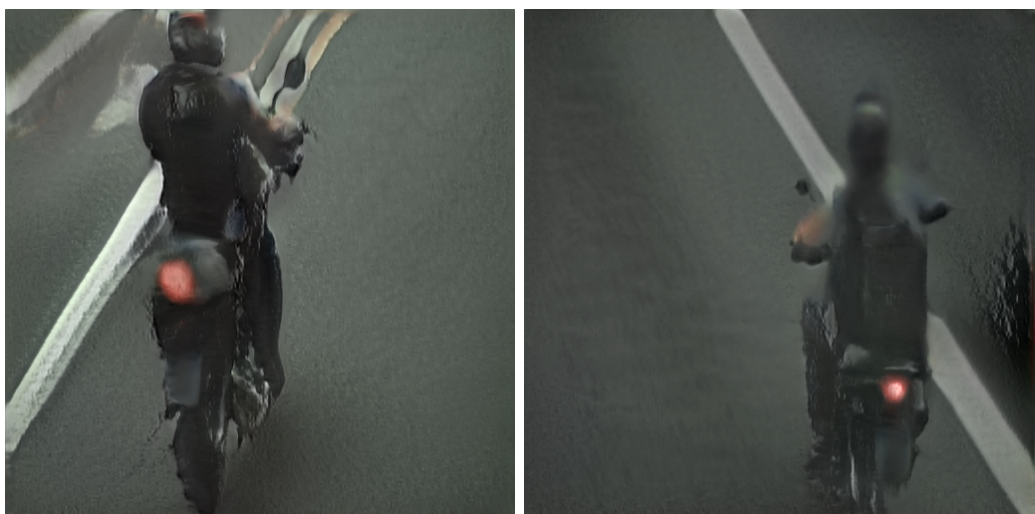


Figure 5.10: Examples of generated images of the *motoribke* class

5.3 Model for object detection and prediction

VGG16

The basic VGG16 model is limited to image classification without bounding box prediction and in this work the basic model is extended with appropriate networks to enable bounding box prediction. The basic model is extended as follows:

- Added a fork to two new deeply connected networks of depth four on the last layer.
- At the output of the first network, an activation function *softmax* [29] with four neurons is added, which is interpreted as assigning the probability that the object belongs to one of the four classes.
- At the output of the second network, a sigmoid activation function with four neurons is added, which is interpreted as assigning relative bounding boxes to the predicted objects.

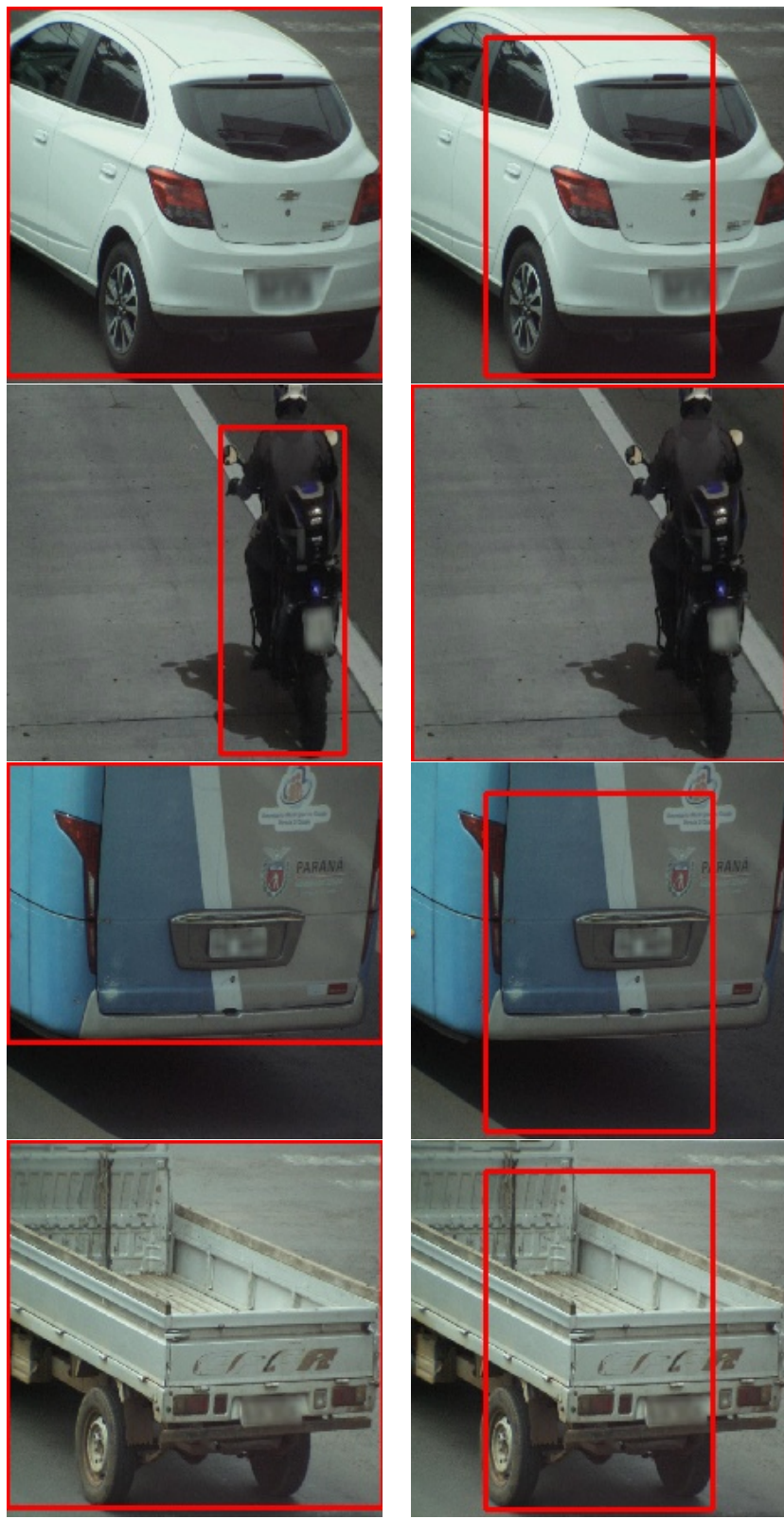
The extended base model was trained on the BVS data set for about ten minutes.

Due to the class imbalance problem that occurs in the BVSdata set, the result of the model is highly biased towards the *car* class, as can be seen from the 5.7 table. The model outputs the bounding boxes incorrectly, as shown in figure 5.11.

Table 5.7: VGG16 model confusion matrix for IoU threshold 0.5 and confidence score threshold for recognized class 0.5

	car	motorbike	bus	truck	no detection
car	85	26	0	1	0
motorbike	0	0	0	0	0
bus	0	0	0	0	0
truck	0	0	0	0	0
no detection	4	71	1	0	0

CHAPTER 5. IMPLEMENTATION AND RESULTS



(a) Actual Frames

(b) Expected frames

Figure 5.11: Example results of the VGG16 model over the test data set

CHAPTER 5. IMPLEMENTATION AND RESULTS

The results of the model evaluation are given in the table 5.8. The results show that the model behaves poorly over the entire data set. Some of the reasons that influence the model to give poor results are the high imbalance between classes and the small amount of available data. The precision of the classes in relation to the IoU threshold is shown in the figure 5.12.

As the basic VGG16 model is extended, there are no freely available corresponding weights of another model that can be used for transfer learning. Using the extended data set BVSstandard or BVSstyle, the amount of data available would still be insufficient. Tens of thousands of images are needed for model training, which are not even available in the extended BVS sets.

Table 5.8: VGG16 model results

class	average precision (eq. 4.6)	macro-averaged F_1 -score (eq. 4.4)
car	0.19	0.58
motorbike	0.0	0.0
bus	0.0	0.0
truck	0.0	0.0
Mean average precision (eq. 4.7)		0.04
Weighted-averaged F_1 - score (eq. 4.5)		0.27

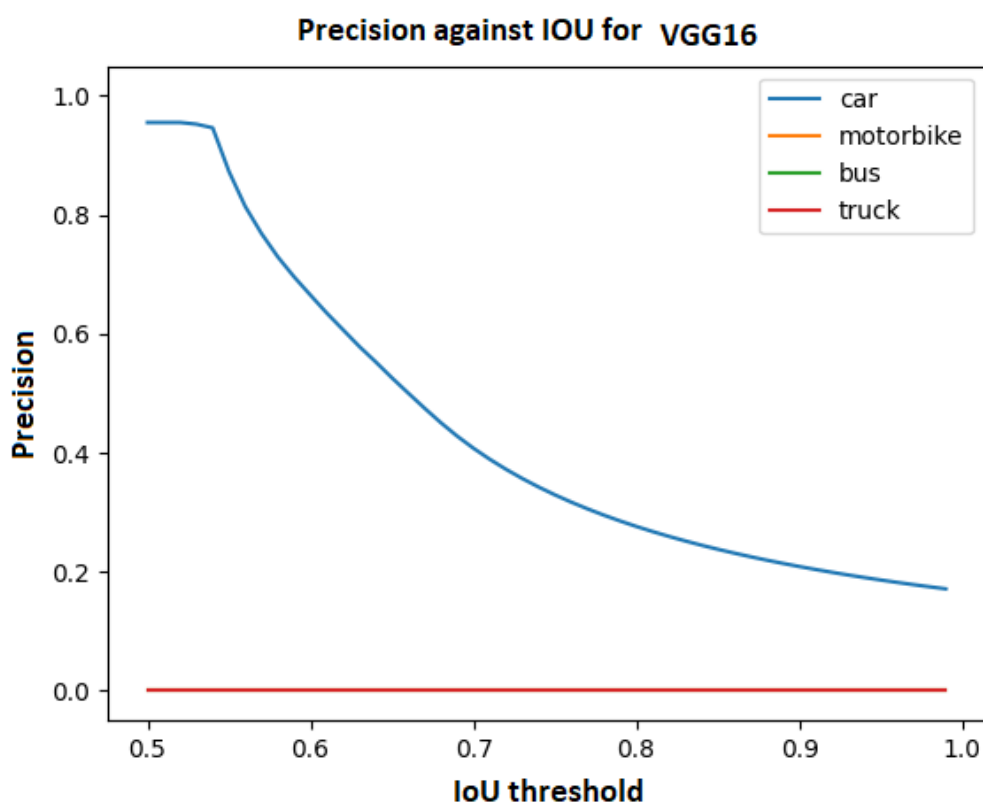


Figure 5.12: Precision in relation to the IoU threshold for the VGG16 model. For classes *motorbike*, *bus* and *truck* the precision in all IoU values is 0.

5.4 YOLO object detection and prediction model

As the VGG16 model cannot provide satisfactory results, the YOLO object detection and prediction model is also considered in the work. Two configurations of the YOLO model are used. The first configuration of the YOLO model serves to compare the results, and is able to predict up to eighty classes. The first configuration is adapted for the COCO dataset. Another configuration of the YOLO model is able to predict up to four classes and is adapted for the BVSdata set.

Prediction of the YOLO model trained on the COCO dataset

The YOLO model is used, which is trained on the COCO dataset containing eighty classes and 328 thousand images. Further in the thesis, the YOLO model trained on the COCO dataset is denoted by $\text{YOLO}_{\text{coco}}$. Model evaluation is performed on the test data set BVS. The confusion matrix was calculated for an IoU threshold value of 0.5 and for a confidence score greater than 0.5. During the calculation of the average precision and macro-averaged F_1 -score, the confidence score of the classes was not taken into account.

From the results of the confusion matrix (table 5.9) and the model evaluation method (table 5.10), the following can be concluded:

- The class *car* is predicted by the $\text{YOLO}_{\text{coco}}$ model with a high precision rating. Eighty-one instances out of a total of eighty-nine are planned. From the confusion matrix, it can be seen that the $\text{YOLO}_{\text{coco}}$ model for three instances had a reliability score of less than 0.5. It also miss-classifies five instances as instances of the *truck* class. The average precision for the *car* class is 0.78, while macro-averaged F_1 -score is 0.91.
- The *motorbike* class is predicted worse than the *car* class. Model $\text{YOLO}_{\text{coco}}$ predicts thirty-seven of the total ninety-seven instances. The majority of instances, forty-nine to be exact, have a value of less than 0.5 for the confidence score. The class confidence scores indicate that the model is not confident in predicting instances from the *motorbike* class. The average precision is 0.27 and macro-averaged F_1 -score is 0.48.
- The *bus* class contains one test image and it is not predicted by the $\text{YOLO}_{\text{coco}}$ model. The average precision and macro-averaged F_1 -score are 0.

CHAPTER 5. IMPLEMENTATION AND RESULTS

- The class *truck* is successfully predicted by the YOLO_{coco} model. The average precision is 1.0 and macro-averaged F_1 -score is 0.99.

Table 5.9: Model confusion matrix YOLO_{coco} for IoU threshold 0.5 and confidence score threshold for recognized class greater than 0.5

	car	motorbike	bus	truck	no detection
car	81	0	0	0	0
motorbike	0	37	0	0	0
bus	0	0	0	0	0
truck	5	0	0	1	0
no detection	3	52	1	0	0

Table 5.10: Results of model evaluation YOLO_{coco}

class	average precision (eq. 4.6)	macro-averaged F_1 -score (eq. 4.4)
car	0.78	0.91
motorbike	0.23	0.48
bus	0.0	0.0
truck	1.0	0.99
Mean average precision (eq. 4.7)		0.50
Weighted-averaged F_1 - score (eq. 4.5)		0.69

The precision of the classes in relation to the IoU threshold is shown in the figure 5.13. The YOLO_{coco} model has a mean average precision (mAP) of 0.50 and weighted-averaged F_1 -score of 0.69. When predicting the YOLO_{coco} model, we can conclude that it recognizes the *car* and *truck* class objects well. The problem observed in predicting those classes is that there are objects that have similar features. Such a problem can be seen in the picture 5.14. The model YOLO_{coco} successfully classified 40% instances of the class *motorbike* from the test set BVS. An instance of the class *bus* is not correctly classified by the YOLO_{coco} model.

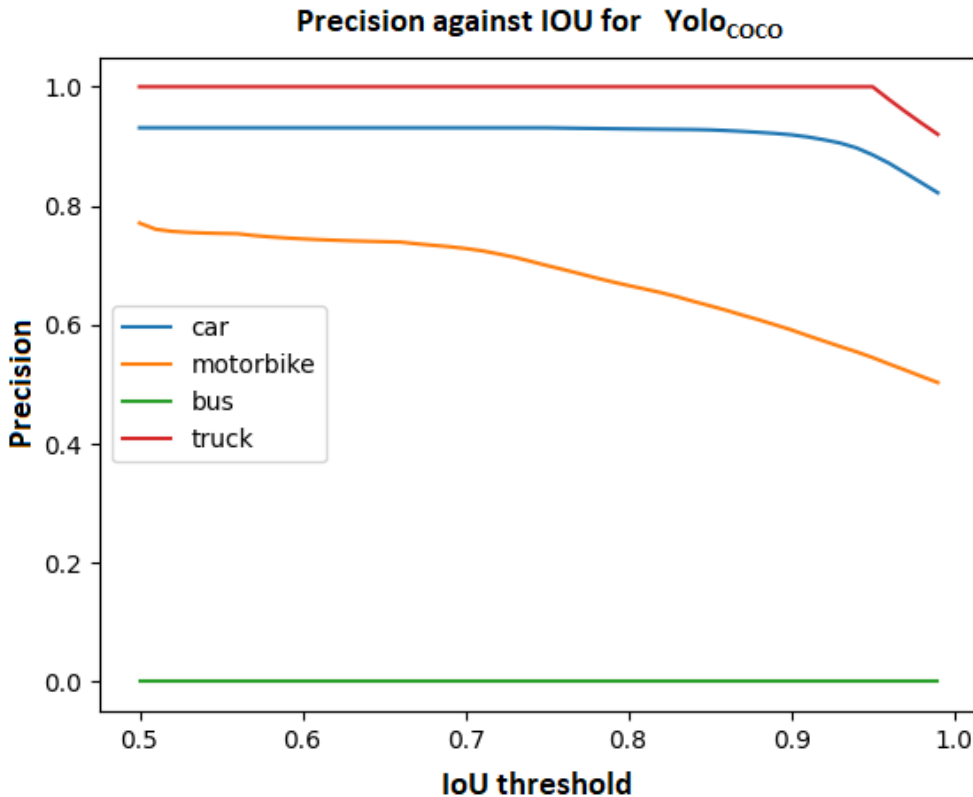


Figure 5.13: Precision in relation to the IoU threshold [0.5,1) of the model YOLO_{coco}

Figure 5.15 shows some predictions of the YOLO_{coco} model. The image shows that some of the objects belonging to the classes *car* (top right), *motorbike* (middle right) and *truck* (bottom left) were successfully detected. In the image belonging to the *motorbike* class (middle left), we can see that the model successfully detected a human, but failed to detect an object of the *motorbike* class, i.e. the confidence score was very low, i.e. was 0.2.



Figure 5.14: Similar features of two different classes, class *car* (left) and class *truck* (right)

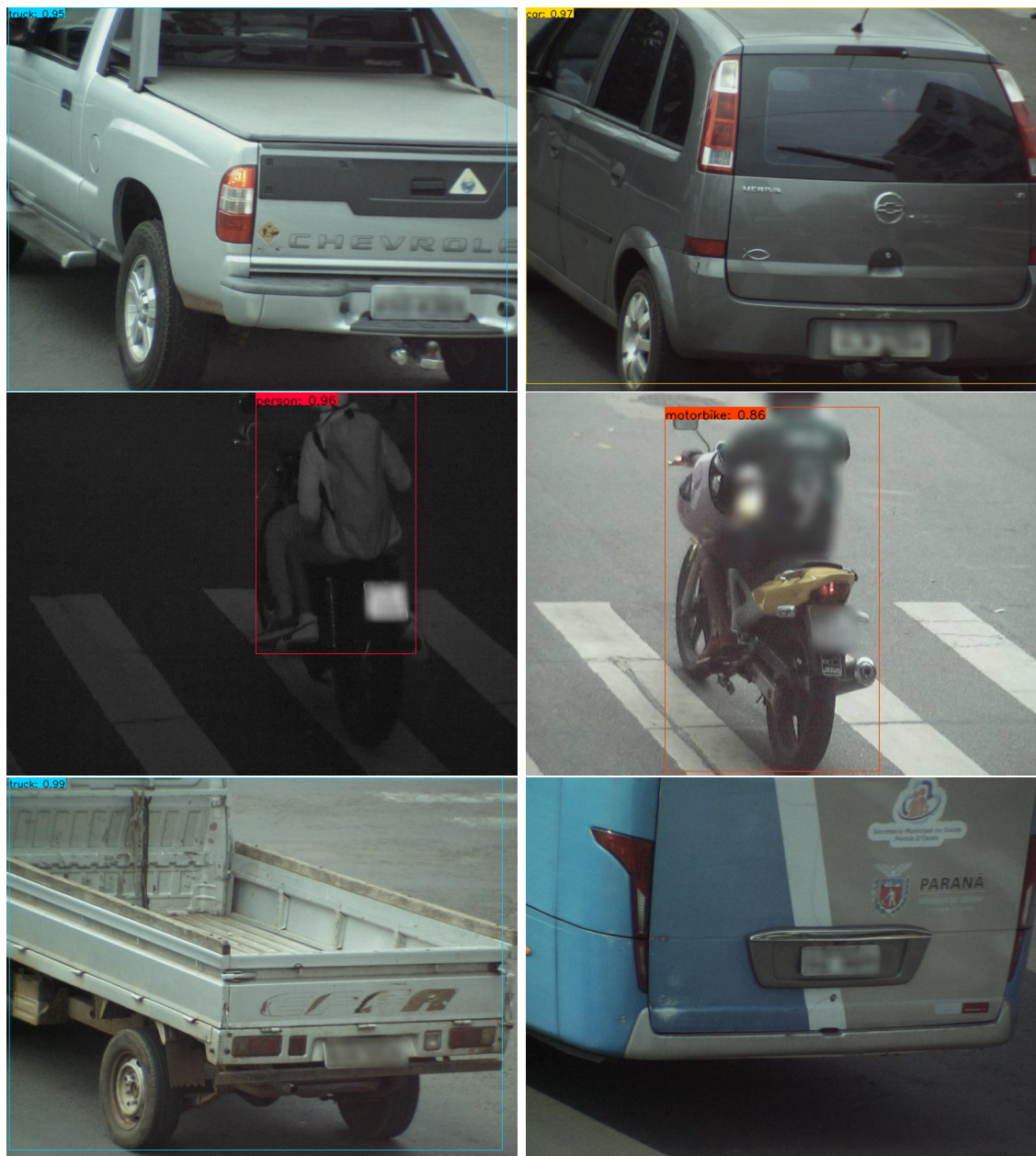


Figure 5.15: Images from the test set and predictions over them by the YOLO_{coco} model, class *car* (top), class *motorbike* (middle), class *truck* (bottom left) and the *bus* class (bottom right). Objects in images without bounding boxes were not successfully detected.

Model training using transfer learning

To improve the results, subsequent models were trained using model weights trained on the COCO dataset. As there is a difference in the number of classes between the BVS dataset and the COCO dataset, some parts of the weights are discarded.

Models are trained on images with a resolution of up to 512×512 . The images are randomly resized from the interval 224×224 to 512×512 , with a step of 32×32 . Model training was limited to one hundred and fifty epochs. The ADAM optimizer with an initial learning rate of $1e^{-3}$ was used to train the model. During model training, the learning rate is multiplied by a factor of 0.9. Also, an early stop flag is set, if the loss function has not decreased in ten consecutive epochs. From the training set, 10% of the validation data was separated.

Model training using transfer learning on the dataset BVS

For object detection, the YOLO model is used, which is trained on the data set BVS, which contains four classes and 1872 images. Further in the thesis, the YOLO model trained on the data set BVS is denoted by YOLO_{BVS} . Figure 5.16 shows the Loss function and learning rate of the YOLO_{BVS} model. It can be seen from the Loss function that the model training stopped early after ninety-nine epochs. The training of the model lasted about two hours.

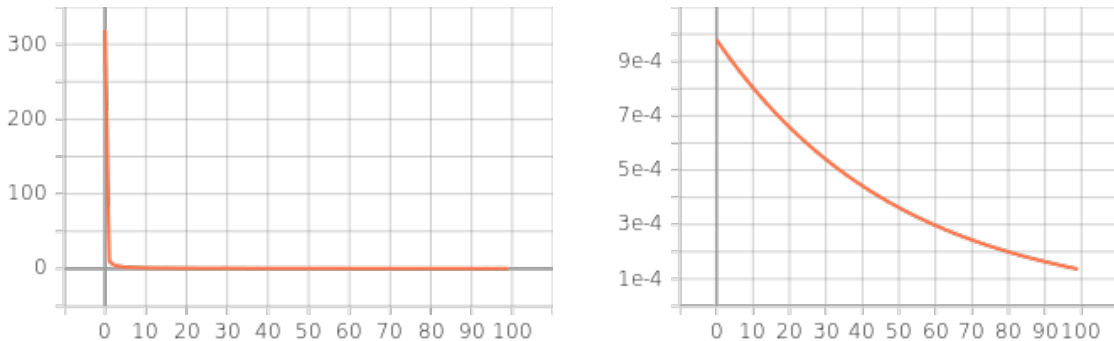


Figure 5.16: Loss function (left) and learning rate (right) of the model YOLO_{BVS} . The x axis represents the number of epochs. The y axis (left) represents the value of the error function. The y axis (right) represents the value for the learning rate.

From the results of the confusion matrix (table 5.11) and the model evaluation method (table 5.12), the following can be concluded:

CHAPTER 5. IMPLEMENTATION AND RESULTS

- class *car* model YOLO_{BVS} successfully predicts in 100% of cases. Eighty-nine out of eighty-nine instances are predicted. The average precision for the *car* class is 0.93 and macro-averaged F_1 -score is 0.99. The
- class *motorbike* is also successfully predicted by the model in 100% cases. The average precision is 0.89 and macro-averaged F_1 -score is 0.99, like class *car*. The
- class *bus* is predicted as an instance of the *motorbike* class. The
- class *truck* is predicted as an instance of the *car* class.

Table 5.11: Model confusion matrix YOLO_{bvs} for IoU threshold 0.5 and confidence score threshold for recognized class 0.5

	car	motorbike	bus	truck	no detection
car	89	0	0	1	0
motorbike	0	97	1	0	0
bus	0	0	0	0	0
truck	0	0	0	0	0
no detection	0	0	0	0	0

Table 5.12: Results of model evaluation YOLO_{bvs}

class	average precision (eq. 4.6)	macro-averaged F_1 -score (eq. 4.4)
car	0.93	0.99
motorbike	0.89	0.99
bus	0.00	0.00
truck	0.00	0.00
Mean average precision (eq. 4.7)		0.46
Weighted-averaged F_1 -score (eq. 4.5)		0.97

The precision of the classes in relation to the IoU threshold is shown in the figure 5.17. The YOLO_{bvs} model has a mean average precision (mAP) of 0.46 and weighted-averaged F_1 -score of 0.97. The mean average precision is lower compared to the YOLO_{coco} model. The weighted-averaged F_1 -score is higher than that of the YOLO_{coco} model, which represents a remarkable improvement. It can be concluded

that the model behaves well in detecting the classes *car* and *motorbike*, while for the class *bus* the prediction is wrong. It can be noted that the problem mentioned in the YOLO_{coco} model still occurs for some instances of the *car* and *truck* classes. An example of the detection results is shown in the figure 5.18. It can be concluded that the YOLO_{BVS} model gives better results than the YOLO_{coco} model.

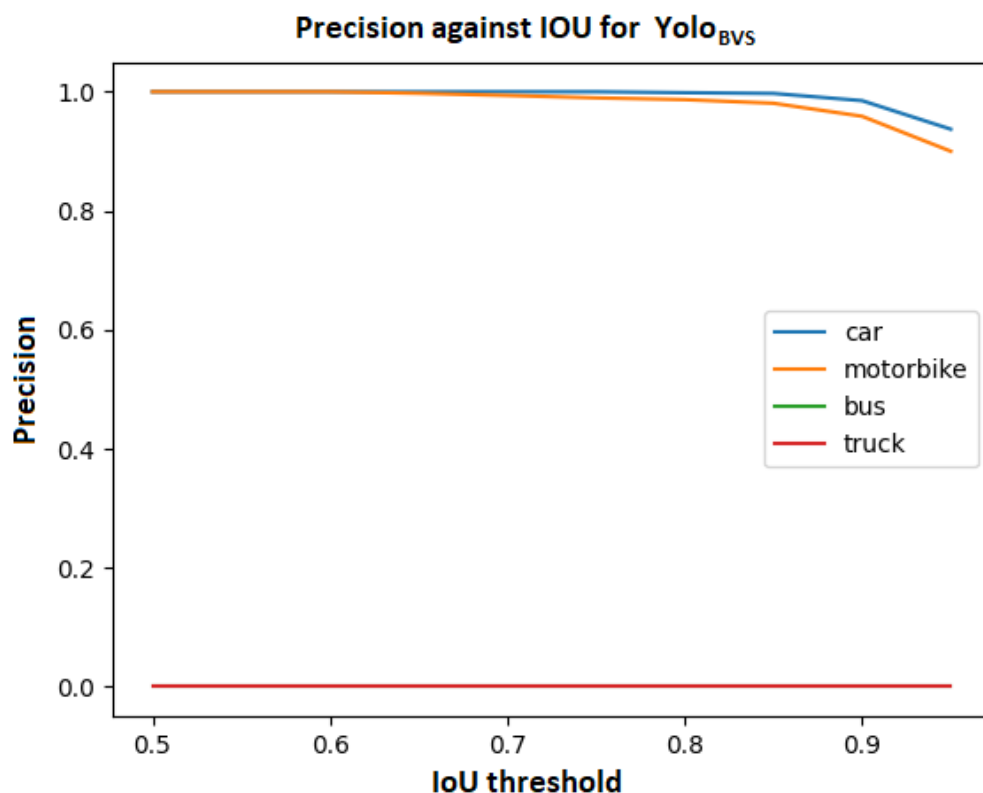


Figure 5.17: Precision in relation to the IoU threshold [0.5,1) of the YOLO_{BVS} model, for classes *bus* and *truck* the precision in all IoU values is 0

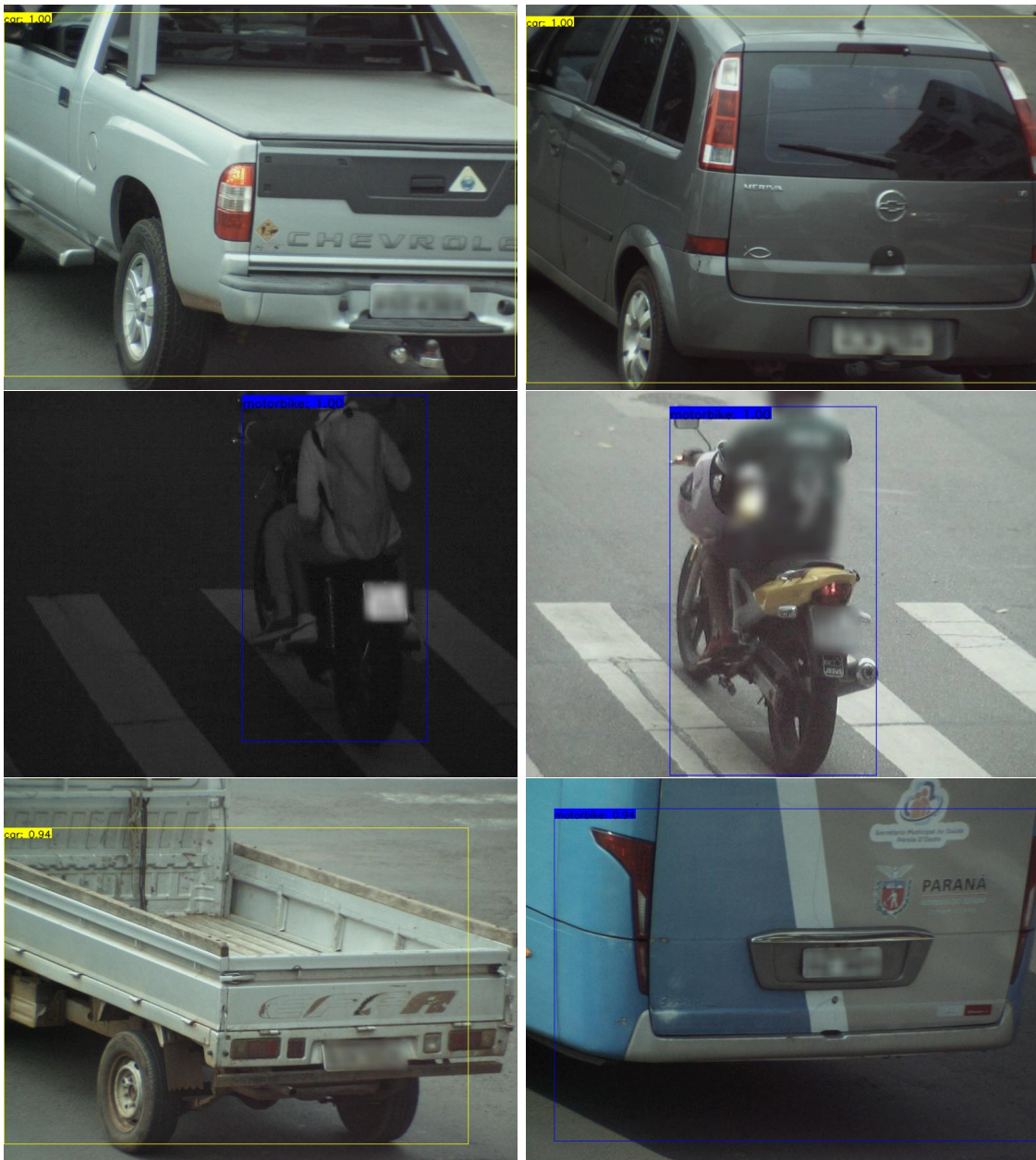


Figure 5.18: Images from the test set and predictions over them by the YOLO_{BVS} model, class *car* (top), class *motorbike* (middle), class *truck* (bottom left) and class *bus* (bottom right)

Model training using transfer learning on dataset BVSstandard

For object detection, the YOLO model is used, which is trained on the BVSstandard data set, which contains four classes and 6952 images. Further in the thesis, the YOLO model trained on the data set BVSstandard is denoted by $\text{YOLO}_{\text{BVSstandard}}$. The model Loss function and learning rate are shown in Fig. 5.19. It can be seen from the Loss function that the model training stopped early after fifty-nine epochs. The model training lasted ten hours.

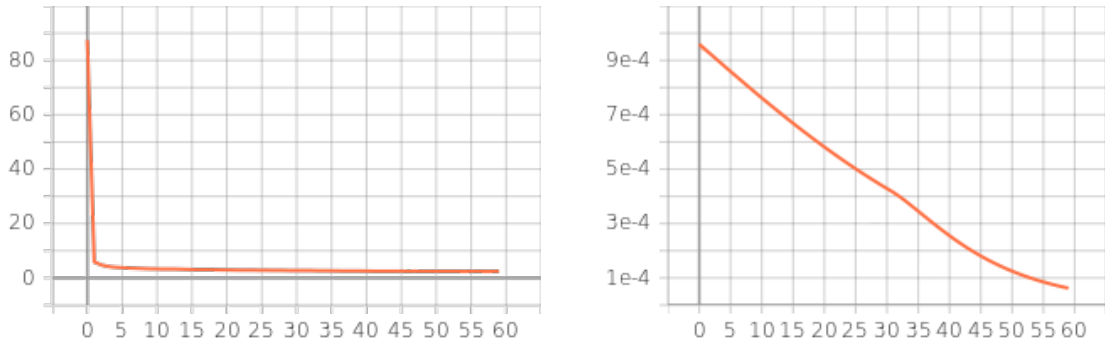


Figure 5.19: Loss function (left) and learning rate (right) of the model $\text{YOLO}_{\text{BVSstandard}}$. The x axis represents the number of epochs. The y axis (left) represents the value of the error function. The y axis (right) represents the value for the learning rate.

From the results of the confusion matrix (table 5.13) and the model evaluation method (table 5.14), the following can be concluded:

- class *car* is predicted by the $\text{YOLO}_{\text{BVSstandard}}$ model in 100% of cases. Eighty-nine out of eighty-nine instances were predicted. The average precision for the *car* class is 0.88, while macro-averaged F_1 -score is 0.99. These results indicate a very good prediction of the $\text{YOLO}_{\text{BVSstandard}}$ model over the *car* class.
- class *motorbike* is predicted as well as class *car*. The $\text{YOLO}_{\text{BVSstandard}}$ model predicts ninety-seven of the ninety-seven instances. The average precision is 0.88 and macro-averaged F_1 -score is 0.99.
- class *bus* is not predicted by the $\text{YOLO}_{\text{BVSstandard}}$ model, more precisely the confidence score is less than 0.5.
- class *truck* is incorrectly predicted as class *car*.

Table 5.13: Model confusion matrix $\text{YOLO}_{\text{BVSstandard}}$ for IoU threshold 0.5 and confidence threshold for recognized class 0.5

	car	motorbike	bus	truck	no detection
car	89	0	0	1	0
motorbike	0	97	0	0	0
bus	0	0	0	0	0
truck	0	0	0	0	0
no detection	0	0	1	0	0

Table 5.14: Model results $\text{YOLO}_{\text{BVSstandard}}$

class	average precision (eq. 4.6)	macro-averaged F_1 -score (eq. 4.4)
car	0.88	0.99
motorbike	0.88	0.99
bus	0.00	0.00
truck	0.00	0.00
Mean average precision (eq. 4.7)		0.44
Weighted-averaged F_1 - score (eq. 4.5)		0.97

The precision of the classes in relation to the IoU threshold is shown in the figure 5.20. The YOLO_{BVSstandard} model has a mean average precision (mAP) of 0.44 and a mean weighted F_1 score of 0.97. When predicting the YOLO_{BVSstandard} model, we can conclude that it recognizes the *car* and *motorbike* class objects well. The mean average precision is lower compared to the YOLO_{coco} model. The results obtained by the YOLO_{BVSstandard} model are very similar to the results of the YOLO_{BVS} model. An example of the detection results is shown in the figure 5.21. It can be concluded that the YOLO_{BVSstandard} model gives better results than the YOLO_{coco} model.

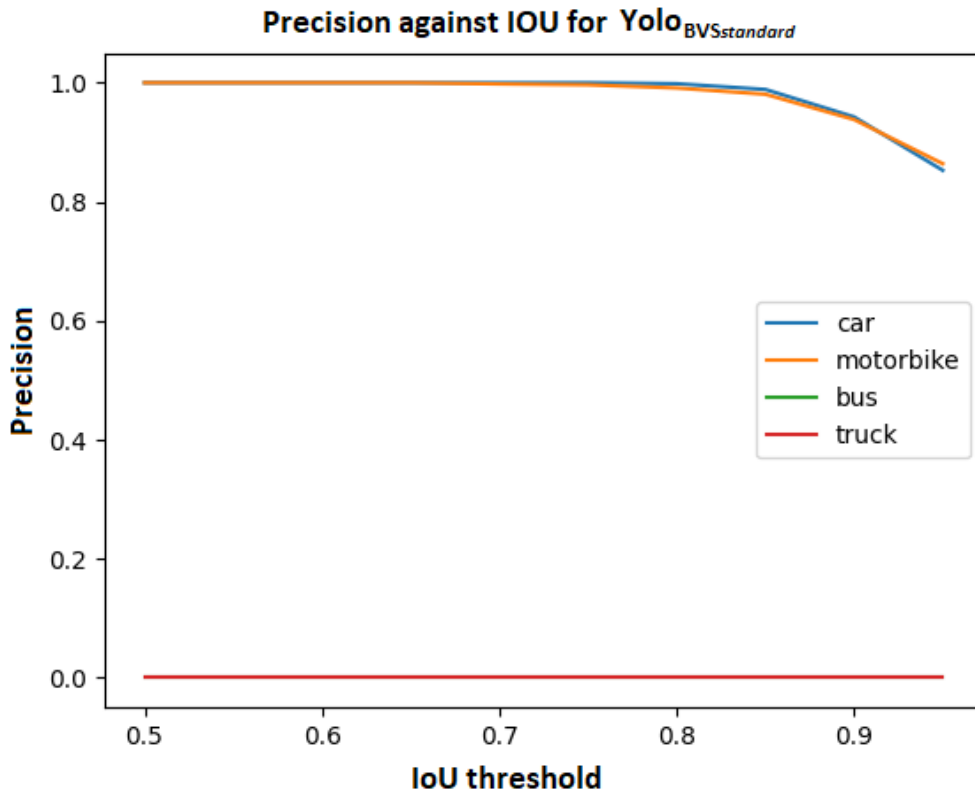


Figure 5.20: Precision relative to the IoU threshold [0.5,1) of the YOLO_{BVSstandard} model. For classes *bus* and *truck* the precision in all IoU values is 0.

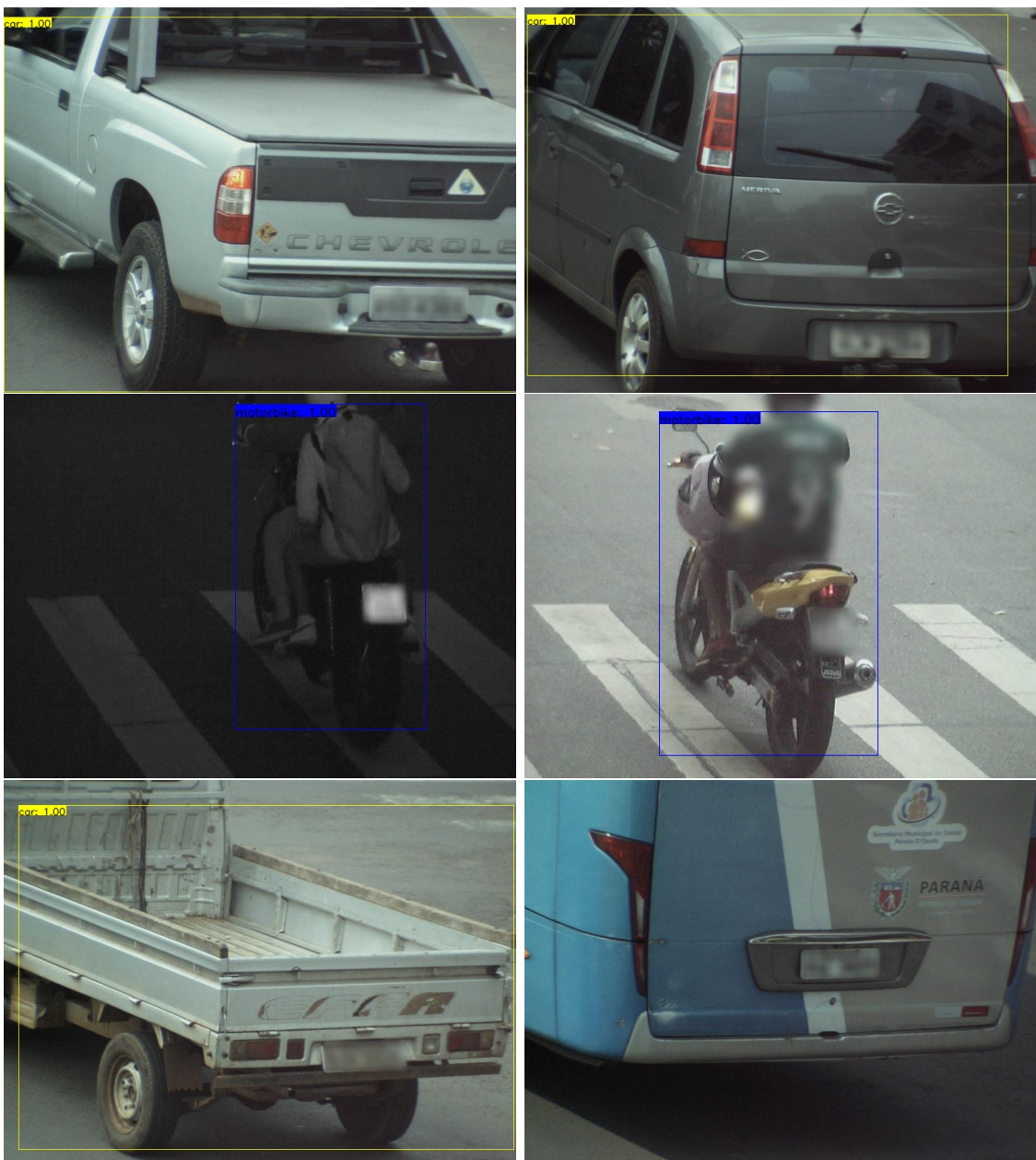


Figure 5.21: Images from the test set and predictions over them by the YOLO_{BVSstandard} model, class *car* (top), class *motorbike* (middle), class *truck* (bottom left) and the *bus* class (bottom right). Objects in images without bounding boxes were not successfully detected.

Model training using transfer learning on a dataset BVSstyle

For object detection, the YOLO model is used, which is trained on the data set BVSstyle, which contains four classes and 6952 images. Further in the thesis, the YOLO model trained on the data set BVSstyle is denoted by $\text{YOLO}_{\text{BVSstyle}}$. The model Loss is shown in the figure 5.22. It can be seen from the Loss function that the model training stopped early after fifty-seven epochs. The training of the model lasted about five hours.

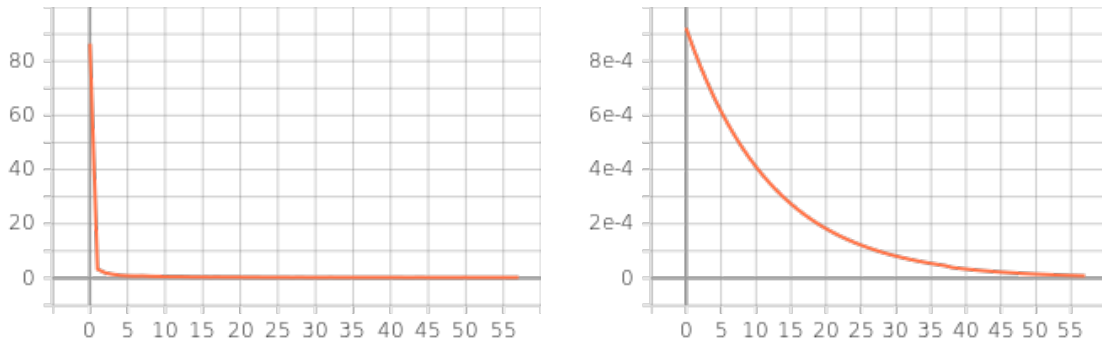


Figure 5.22: Loss function (left) and learning rate (right) of the model $\text{YOLO}_{\text{BVSstyle}}$. The x axis represents the number of epochs. The y axis (left) represents the value of the error function. The y axis (right) represents the value for the learning rate.

From the results of the confusion matrix (table 5.15) and the model evaluation method (table 5.16), the following can be concluded:

- class *car* model $\text{YOLO}_{\text{BVSstyle}}$ predicts in 100% of cases. Eighty-nine out of eighty-nine instances were predicted. The average precision for the *car* class is 0.88, while macro-averaged F_1 -score is 0.99. These results indicate a perfect prediction of the $\text{YOLO}_{\text{BVSstyle}}$ model over the *car* class. The
- class *motorbike* is predicted as well as the *car* class. Model $\text{YOLO}_{\text{BVSstyle}}$ predicts ninety-seven of the ninety-seven instances. The average precision is 0.82 and macro-averaged F_1 -score is 0.98.
- class *bus* model $\text{YOLO}_{\text{BVSstyle}}$ successfully predicts. The average precision and macro-averaged F_1 -score are 1.00.
- class *truck* is incorrectly predicted as class *car*.

Table 5.15: Model confusion matrix YOLO_{BVSstyle} for IoU threshold 0.5 and confidence threshold for recognized class 0.5

	car	motorbike	bus	truck	no detection
car	89	0	0	1	0
motorbike	0	97	0	0	0
bus	0	0	1	0	0
truck	0	0	0	0	0
no detection	0	0	0	0	0

Table 5.16: Model results YOLO_{BVSstyle}

class	average precision (eq. 4.6)	macro-averaged F_1 -score (eq. 4.4)
car	0.88	0.99
motorbike	0.82	0.98
bus	1.00	1.00
truck	0.00	0.00
Mean average precision (eq. 4.7)		0.68
Weighted-averaged F_1 - score (eq. 4.5)		0.98

CHAPTER 5. IMPLEMENTATION AND RESULTS

The precision of the classes in relation to the IoU threshold is shown in the figure 5.23. Model YOLO_{BVS^{style}} has mean average precision (mAP), which is 0.68. The mean average precision is the highest compared to all YOLO models. The weighted-averaged F_1 -score is 0.98 and it also represents the best result obtained. When predicting the YOLO_{BVS^{style}} model, we can conclude that it predicts objects of the *car*, *motorbike* and *bus* classes well. The YOLO_{BVS^{style}} model gives the best results. The loss, as with the YOLO_{BVS^{standard}} and YOLO_{BVS} models, occurs in the prediction of the *truck* class. An example of detection results is shown in the figure 5.24. It can be concluded that the YOLO_{BVS^{style}} model gives the best results.

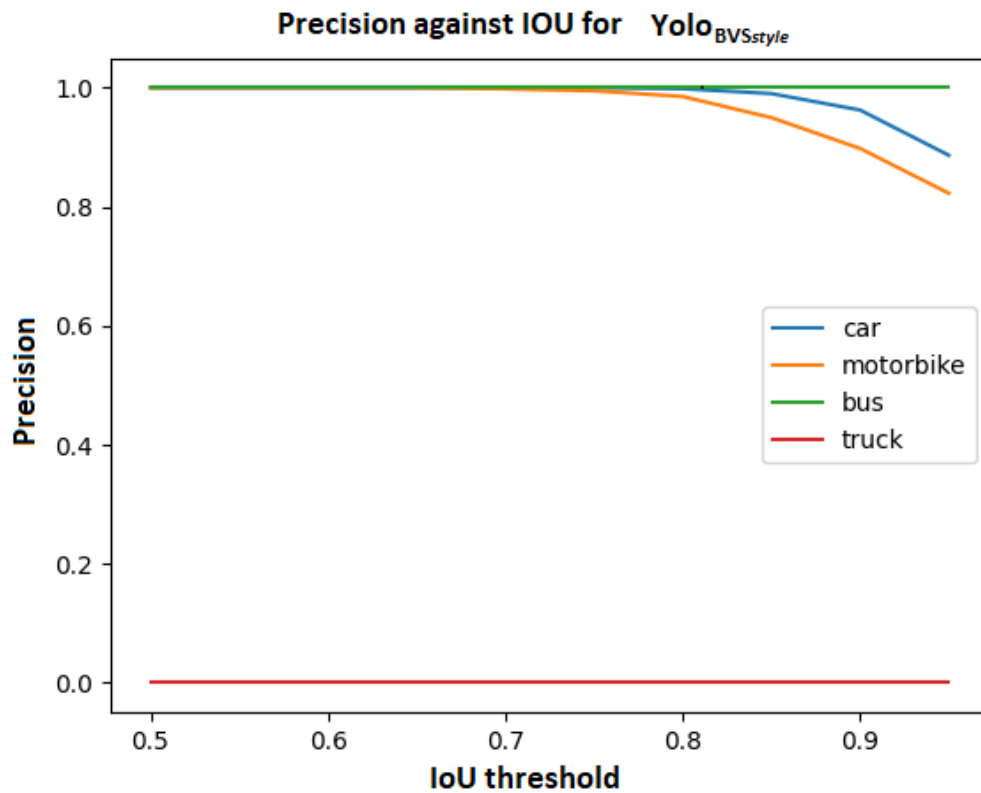


Figure 5.23: Precision in relation to the IoU threshold [0.5,1) of the model YOLO_{BVS^{style}}

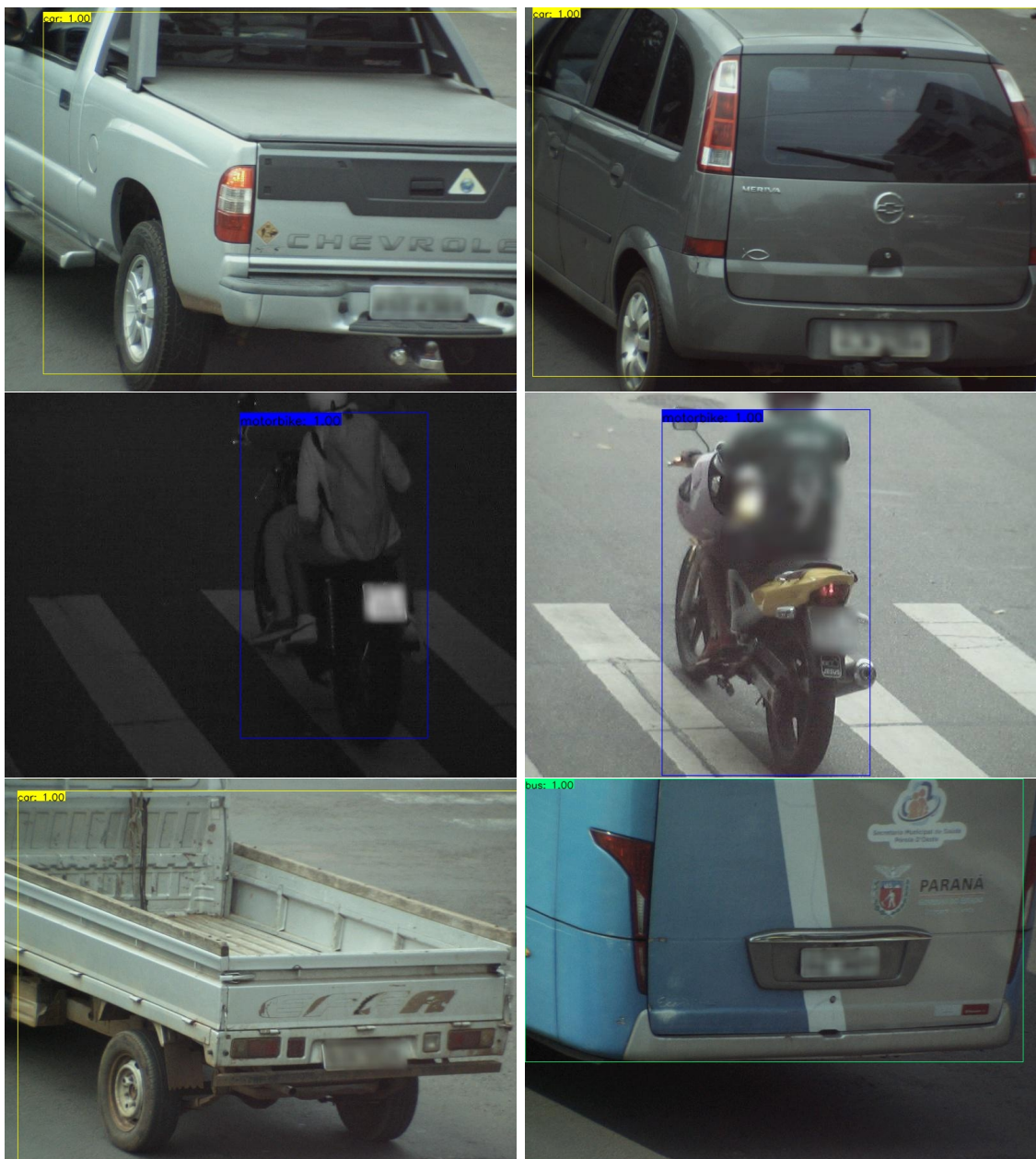


Figure 5.24: Images from the test set and predictions over them by the $\text{YOLO}_{\text{BVSstyle}}$ model, class *car* (top), class *motorbike* (middle), class *truck* (bottom left) and class *bus* (bottom right).

5.5 Comparative analysis of results

Model VGG16 was trained on BVSdata, while the YOLO model was trained on BVS, BVSstandard and BVSstyle separately, and the following results were obtained, which are shown in the table 5.17.

Table 5.17: Results of trained object detection models

	Mean average precision (eq. 4.7)	Weighted-averaged F_1 -score (eq. 4.5)
VGG16	0.04	0.27
YOLO _{coco}	0.50	0.69
YOLO _{BVS}	0.45	0.97
YOLO _{BVSstandard}	0.44	0.97
YOLO _{BVSstyle}	0.68	0.98

Based on the mean average precision, for the models listed in the table 5.17 it can be observed that the best results are given by the model YOLO_{BVSstyle}, while the VGG16 model does not give satisfactory results. Some of the reasons that influence the VGG16 model to give unsatisfactory results are the high imbalance between classes and the small amount of available data. As for the YOLO_{BVS} and YOLO_{BVSstandard} models, which give the same results for the evaluation metrics, there is insufficient improvement in the YOLO_{BVSstandard} compared to the YOLO_{BVS} model. Namely, it is possible that there was an insufficient improvement in the recognition of the instance of the class *bus*, but the confidence score did not exceed the set threshold (0.5).

Chapter 6

Conclusion

In this thesis, the problem of expanding the data set used for training models for object detection is solved. The dataset is expanded with images obtained by standard transformations (translation, rotation, color change, etc.) and synthetically generated images by generative adversarial networks. In total, about five thousand images were added to the dataset. The thus expanded data sets, BVSstandard and BVSstyle, were separately used to train the YOLO object detection model, while the VGG16 model was trained on the original BVSdata set.

In order to improve the results of the YOLO model, training with knowledge transfer was used. The model weights used were trained on the COCO dataset.

The results obtained after training the YOLO model on the BVS, BVSstandard and BVSstyle datasets are better than the results obtained with the VGG16 model. For the YOLO models trained on the BVS, BVSstandard and BVSstyle datasets, it can be concluded from the results that the precision has improved for the *car* and *motorbike* classes compared to $\text{YOLO}_{\text{COCO}}$ model. For the YOLO models trained on the BVS and BVSstandard datasets, the mean average precision dropped because the *truck* class is no longer recognized, which may be the cause of sharing features with the class *car*. The YOLO model trained on the BVSstyle dataset also successfully predicts the *bus* class. It can be concluded that the $\text{YOLO}_{\text{BVSstyle}}$ model gives the best results.

Better results for object detection can be obtained by increasing the amount of data available to *StyleGAN2* models and training them for a longer period of time. This expands the training set with higher quality and more diverse images generated by the *StyleGAN2* model. Enhancement can also be achieved by using the union of the BVSstandard and BVSstyle datasets.

CHAPTER 6. CONCLUSION

Thanks to the development of new technologies, it may be possible to generate synthetic data using entirely new methods. For example, the *DALL-E 2* [42] and *MidJourney* [43] models are able to generate realistic images based on their textual descriptions. This approach, however, requires new data, i.e. textual descriptions of images.

Bibliography

- [1] Yoshua Bengio, Yann LeCun, et al. Scaling learning algorithms towards ai. *Large-scale kernel machines*, 34(5):1–41, 2007.
- [2] Geert Litjens, Thijs Kooi, Babak Ehteshami Bejnordi, Arnaud Arindra Adiyoso Setio, Francesco Ciompi, Mohsen Ghafoorian, Jeroen Awm Van Der Laak, Bram Van Ginneken, and Clara I Sánchez. A survey on deep learning in medical image analysis. *Medical image analysis*, 42:60–88, 2017.
- [3] Fuzhen Zhuang, Zhiyuan Qi, Keyu Duan, Dongbo Xi, Yongchun Zhu, Hengshu Zhu, Hui Xiong, and Qing He. A comprehensive survey on transfer learning. *Proceedings of the IEEE*, 109(1):43–76, 2020.
- [4] Alexey Bochkovskiy, Chien-Yao Wang, and Hong-Yuan Mark Liao. Yolov4: Optimal speed and accuracy of object detection. *arXiv preprint arXiv:2004.10934*, 2020.
- [5] Yoshua Bengio. Deep learning of representations for unsupervised and transfer learning. In *Proceedings of ICML workshop on unsupervised and transfer learning*, pages 17–36. JMLR Workshop and Conference Proceedings, 2012.
- [6] Lorenzo Brigato and Luca Iocchi. A close look at deep learning with small data. In *2020 25th International Conference on Pattern Recognition (ICPR)*, pages 2490–2497. IEEE, 2021.
- [7] Lanlan Liu, Michael Muelly, Jia Deng, Tomas Pfister, and Li-Jia Li. Generative modeling for small-data object detection. In *Proceedings of the IEEE/CVF International Conference on Computer Vision*, pages 6073–6081, 2019.
- [8] Shengyu Zhao, Zhijian Liu, Ji Lin, Jun-Yan Zhu, and Song Han. Differentiable augmentation for data-efficient gan training. *Advances in Neural Information Processing Systems*, 33:7559–7570, 2020.

BIBLIOGRAPHY

- [9] Dana H Ballard and Christopher M Brown. Computer vision. englewood cliffs. *J: Prentice Hall*, 1982.
- [10] Thomas Huang. Computer vision: Evolution and promise. 1996.
- [11] Connor Shorten and Taghi M Khoshgoftaar. A survey on image data augmentation for deep learning. *Journal of big data*, 6(1):1–48, 2019.
- [12] Zhengxia Zou, Zhenwei Shi, Yuhong Guo, and Jieping Ye. Object detection in 20 years: A survey. *arXiv preprint arXiv:1905.05055*, 2019.
- [13] Ross Girshick, Jeff Donahue, Trevor Darrell, and Jitendra Malik. Rich feature hierarchies for accurate object detection and semantic segmentation. In *Proceedings of the IEEE conference on computer vision and pattern recognition*, pages 580–587, 2014.
- [14] Shaoqing Ren, Kaiming He, Ross Girshick, and Jian Sun. Faster r-cnn: Towards real-time object detection with region proposal networks. *Advances in neural information processing systems*, 28, 2015.
- [15] Kai Kang, Hongsheng Li, Junjie Yan, Xingyu Zeng, Bin Yang, Tong Xiao, Cong Zhang, Zhe Wang, Ruohui Wang, Xiaogang Wang, et al. T-cnn: Tubelets with convolutional neural networks for object detection from videos. *IEEE Transactions on Circuits and Systems for Video Technology*, 28(10):2896–2907, 2017.
- [16] Yali Amit, Pedro Felzenszwalb, and Ross Girshick. Object detection. *Computer Vision: A Reference Guide*, pages 1–9, 2020.
- [17] Karen Simonyan and Andrew Zisserman. Very deep convolutional networks for large-scale image recognition. *arXiv preprint arXiv:1409.1556*, 2014.
- [18] Imagenet challange. <https://image-net.org/challenges/LSVRC/2013/>.
- [19] Deepthi Narayan, Srikanta Murthy, and G Hemantha Kumar. Image segmentation based on graph theoretical approach to improve the quality of image segmentation. *International Journal of Computer and Information Engineering*, 2(6):1803–1806, 2008.

BIBLIOGRAPHY

- [20] Jasper RR Uijlings, Koen EA Van De Sande, Theo Gevers, and Arnold WM Smeulders. Selective search for object recognition. *International journal of computer vision*, 104(2):154–171, 2013.
- [21] Rohith Gandhi. R-cnn, fast r-cnn, faster r-cnn, yolo - object detection algorithms, Jul 2018.
- [22] Ross Girshick. Fast r-cnn. In *Proceedings of the IEEE international conference on computer vision*, pages 1440–1448, 2015.
- [23] Joseph Redmon, Santosh Divvala, Ross Girshick, and Ali Farhadi. You only look once: Unified, real-time object detection. In *Proceedings of the IEEE conference on computer vision and pattern recognition*, pages 779–788, 2016.
- [24] Jalel Ktari, Tarek Frikha, Monia Hamdi, Hela Elmannai, and Habib Hmam. Lightweight ai framework for industry 4.0 case study: Water meter recognition. *Big Data and Cognitive Computing*, 6(3), 2022.
- [25] Mae Mu. Orange fruit photo, 2019. [Online; accessed August 16, 2022].
- [26] Andelka Zečević Mladen Nikolić. *Naučno izračunavanje*. Beograd, 2019.
- [27] Ian Goodfellow, Jean Pouget-Abadie, Mehdi Mirza, Bing Xu, David Warde-Farley, Sherjil Ozair, Aaron Courville, and Yoshua Bengio. Generative adversarial nets. *Advances in neural information processing systems*, 27, 2014.
- [28] Jie Feng, Xueliang Feng, Jiantong Chen, Xianghai Cao, Xiangrong Zhang, Licheng Jiao, and Tao Yu. Generative adversarial networks based on collaborative learning and attention mechanism for hyperspectral image classification, 2020.
- [29] Andelka Zečević Mladen Nikolić. *Mašinsko učenje*. Beograd, 2019.
- [30] Ian Goodfellow, Jean Pouget-Abadie, Mehdi Mirza, Bing Xu, David Warde-Farley, Sherjil Ozair, Aaron Courville, and Yoshua Bengio. Generative adversarial networks. *Communications of the ACM*, 63(11):139–144, 2020.
- [31] Geoffrey M Hodgson. Microeconomics: Behavior, institutions, and evolution, samuel bowles, princeton university press and russell sage foundation, 2004, 584 pages. *Economics & Philosophy*, 22(1):166–171, 2006.

BIBLIOGRAPHY

- [32] Tero Karras, Timo Aila, Samuli Laine, and Jaakko Lehtinen. Progressive growing of gans for improved quality, stability, and variation. *arXiv preprint arXiv:1710.10196*, 2017.
- [33] Tero Karras, Samuli Laine, and Timo Aila. A style-based generator architecture for generative adversarial networks. In *Proceedings of the IEEE/CVF conference on computer vision and pattern recognition*, pages 4401–4410, 2019.
- [34] Xun Huang and Serge Belongie. Arbitrary style transfer in real-time with adaptive instance normalization. In *Proceedings of the IEEE international conference on computer vision*, pages 1501–1510, 2017.
- [35] Tero Karras, Samuli Laine, Miika Aittala, Janne Hellsten, Jaakko Lehtinen, and Timo Aila. Analyzing and improving the image quality of stylegan. In *Proceedings of the IEEE/CVF conference on computer vision and pattern recognition*, pages 8110–8119, 2020.
- [36] Yutaka Sasaki et al. The truth of the f-measure. *Teach tutor mater*, 1(5):1–5, 2007.
- [37] Martin Heusel, Hubert Ramsauer, Thomas Unterthiner, Bernhard Nessler, and Sepp Hochreiter. Gans trained by a two time-scale update rule converge to a local nash equilibrium. *Advances in neural information processing systems*, 30, 2017.
- [38] DC Dowson and BV666017 Landau. The fréchet distance between multivariate normal distributions. *Journal of multivariate analysis*, 12(3):450–455, 1982.
- [39] Nikola Grulovic. Vehicle detection github, 2022. Available at <https://github.com/Grula/vehicle-detection>.
- [40] Nikola Grulovic. Vehicle detection data, 2022. Available at <https://drive.google.com/file/d/1Ekr028-iBCVWyPqy5mJXn8P8EoKQ6xUH/view?usp=sharing>.
- [41] Shengyu Zhao, Zhijian Liu, Ji Lin, Jun-Yan Zhu, and Song Han. Data-efficient gans with diffaugment. Technical report, 2020.
- [42] Mr D Murahari Reddy, Mr Sk Masthan Basha, Mr M Chinnaiahgari Hari, and Mr N Penchalaiah. Dall-e: Creating images from text. *UGC Care Group I Journal*, 8(14):71–75, 2021.

BIBLIOGRAPHY

[43] Jack Daniel, Max. midjourney creating images from text, 2022.

Biography of the author

Nikola Grulović (*Belgrade, Serbia, July 14, 1993*) graduated in Computer Science from the University of Belgrade. He graduated from the “Fifth Belgrade High School”, majoring in natural sciences in 2012 in Belgrade. He entered the Faculty of Mathematics in Belgrade in 2013, majoring in Informatics and graduated in September 2018. After completing his academic studies, he enrolled in master’s studies, and during the 2019-2020 academic year, he passed all the exams provided for in the plan and program of master’s studies. In the period from November 2020 to April 2022, he worked as an intern at *AM Energia*, Sorocaba, Brazil. During his internship, he worked on improving existing systems and upgrading systems with new technologies.